Chapter 2: Roles of Atmosphere-Ocean Interactions in Shaping Tropical Mean Climate

2.1 Latitudinal asymmetry of ITCZ

Major references:

Mitchell, T. P. and J.M. Wallace, 1992:*The annual cycle in equatorial convection and sea surface temperature. Journal of Climate, 1140-1156*

Chang, P. and S.G. Philander, 1994: *A coupled ocean-atmosphere instability of relevance to the seasonal cycle. J.Atmos.Sci.*

Xie, S.P. and S.G. Philander, 1994: *A coupled ocean-atmosphere model of relevance to the ITCZ in the eastern Pacific. Tellus.*

Philander et al. 1996: Why the ITCZ is mostly north of the equator. J. Climate, 9, 2958-2972.

Li 1997: Air-sea interactions of relevance to the ITCZ: the analysis of coupled instabilities and experiments in a hybrid coupled GCM. *J. Atmos. Sci*., **54**, 134-147.

1. Observational features

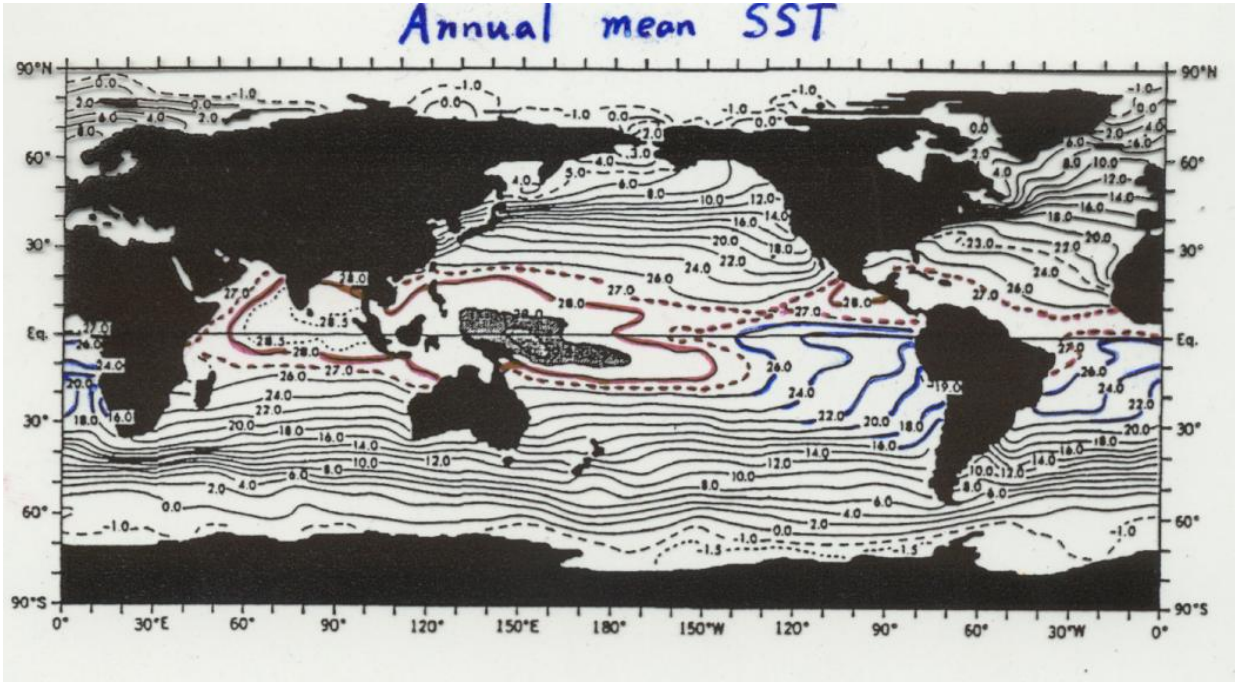
Annual mean SST
90°N
60°
30°
Eq.
30°
60°
90°S
0°
30°E
60°
90°
120°
150°E
180°
150°W
120°
90°
60°
30°W
0°

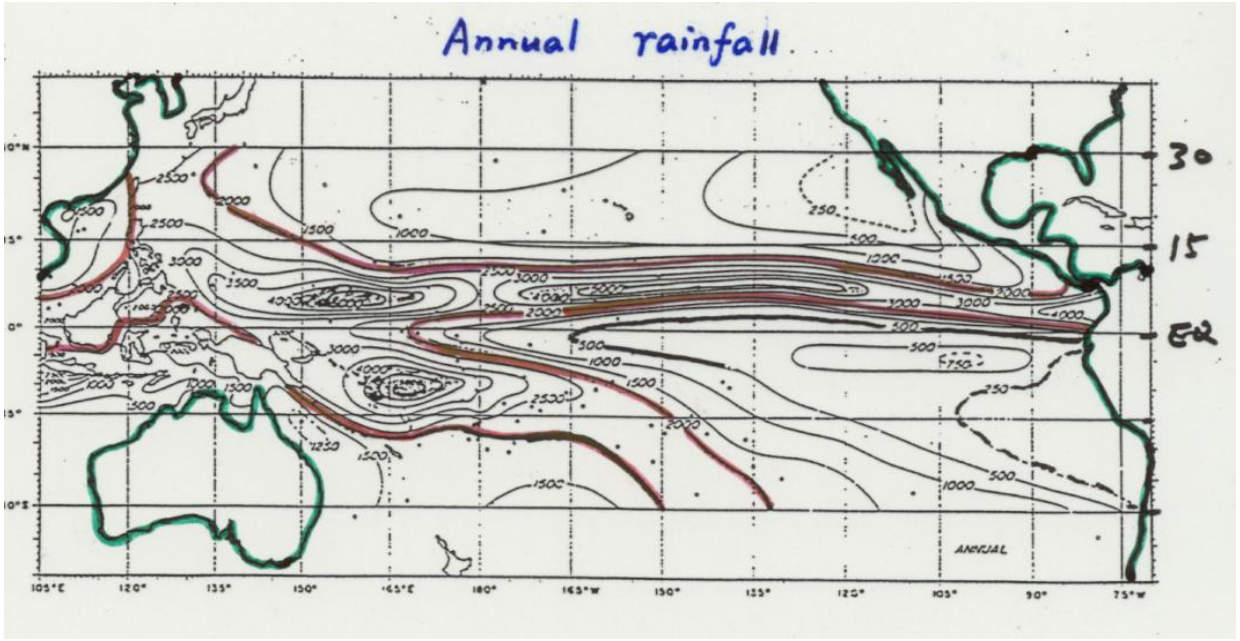
Annual rainfall
30
15
ANNUAL

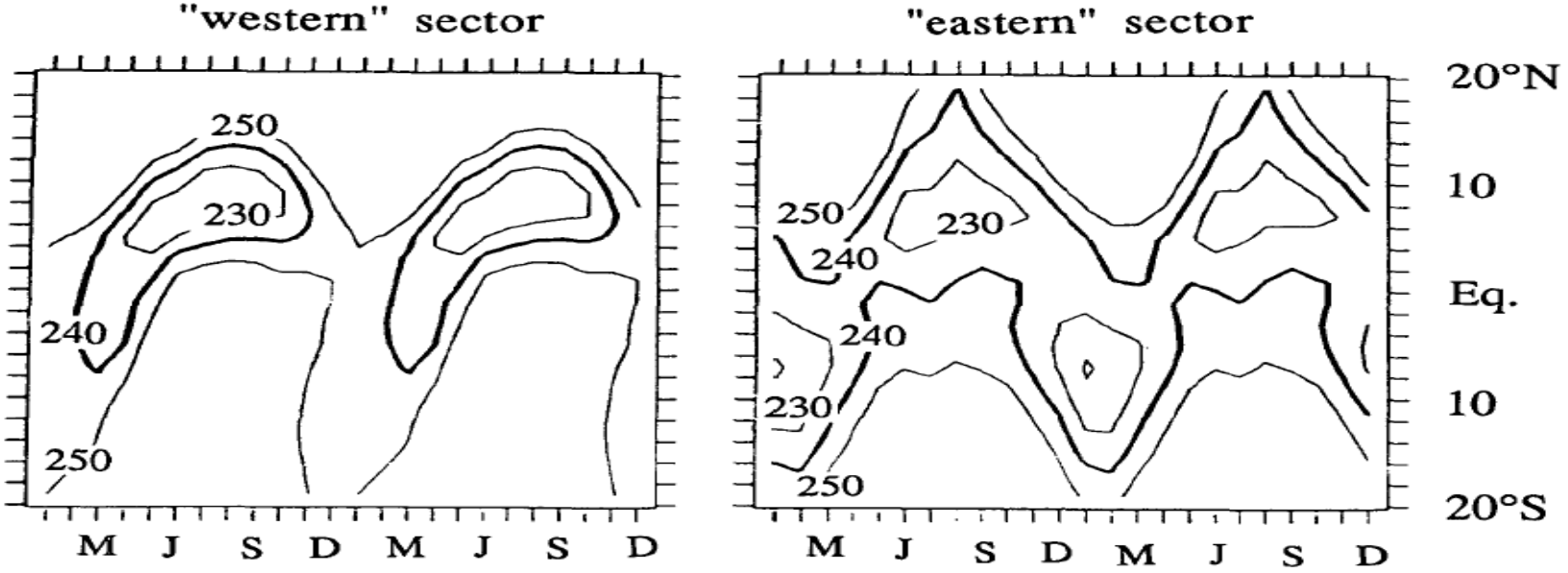

FIG. 3. As in Fig. 1 but for zonal mean OLR for (a) the "western" sector, which includes the eastern Pacific Ocean (140°W), South America, the Atlantic Ocean, and Africa (40°E), and (b) the "eastern" sector, which includes the Indian Ocean (40°E), Indonesia, and the western and central Pacific Ocean (140°W). Contour interval is 10 W m^{-2}.

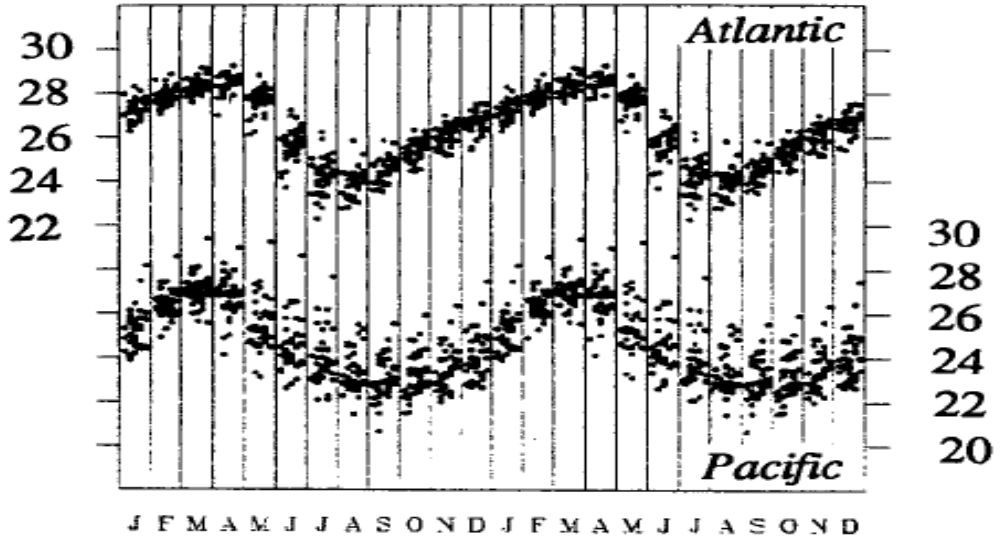

FIG. 4. Scatterdiagram of monthly mean SST (degrees Celcius) for the equatorial cold tongue region of the Atlantic (4°N–4°S, 16°W–4°E) and Pacific (4°N–4°S, 104–86°W) oceans, grouped by calendar month. The dots within each month are staggered, and the calendar year is repeated.

Observed evolution feature (May – March)

(Mitchell and Wallace 1992)

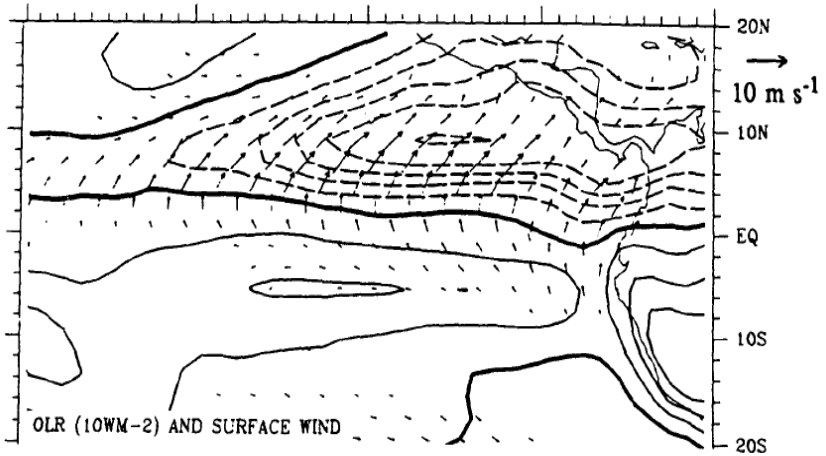

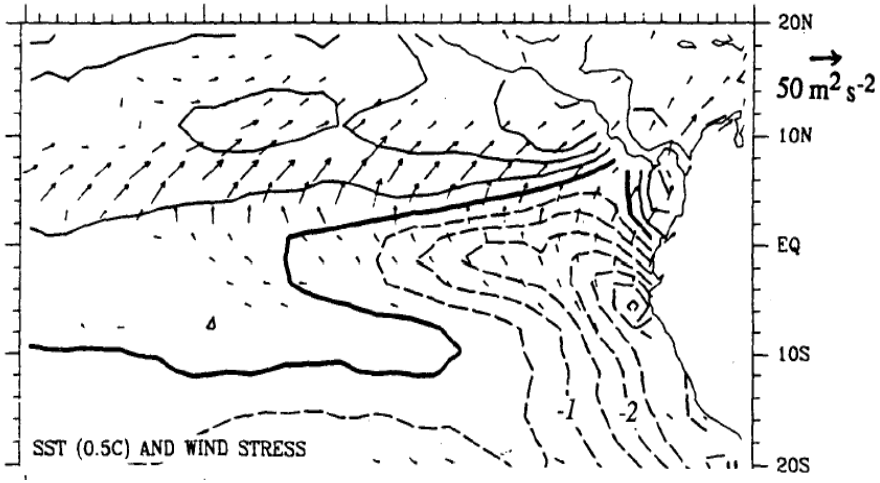

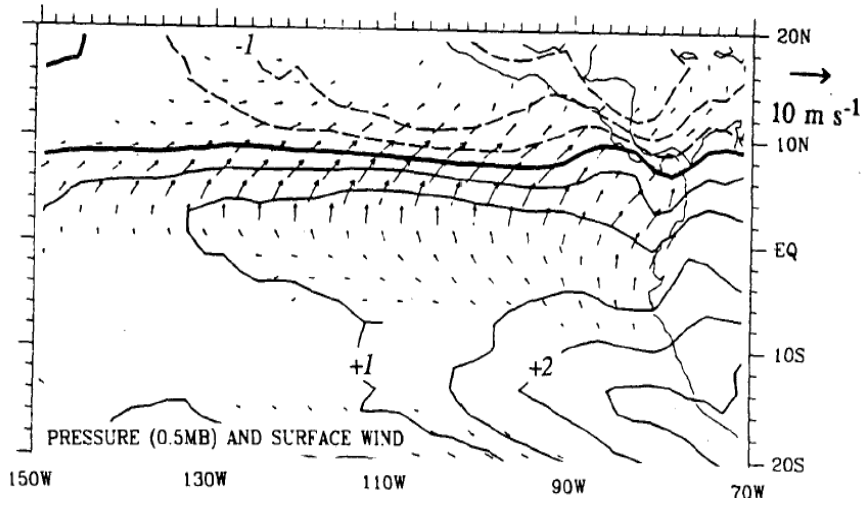

Observed evolution feature (August – May)

(Mitchell and Wallace 1992)

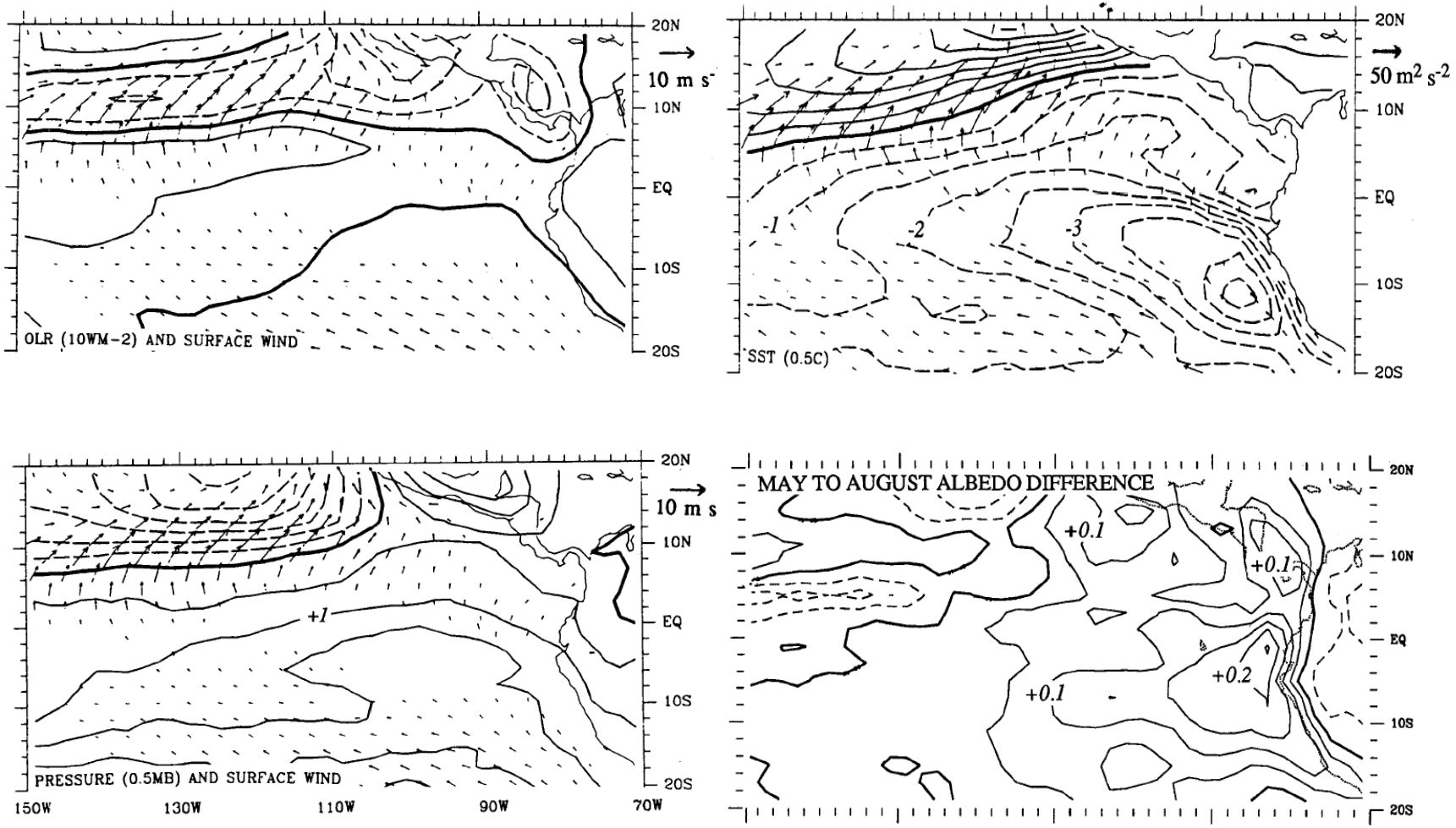

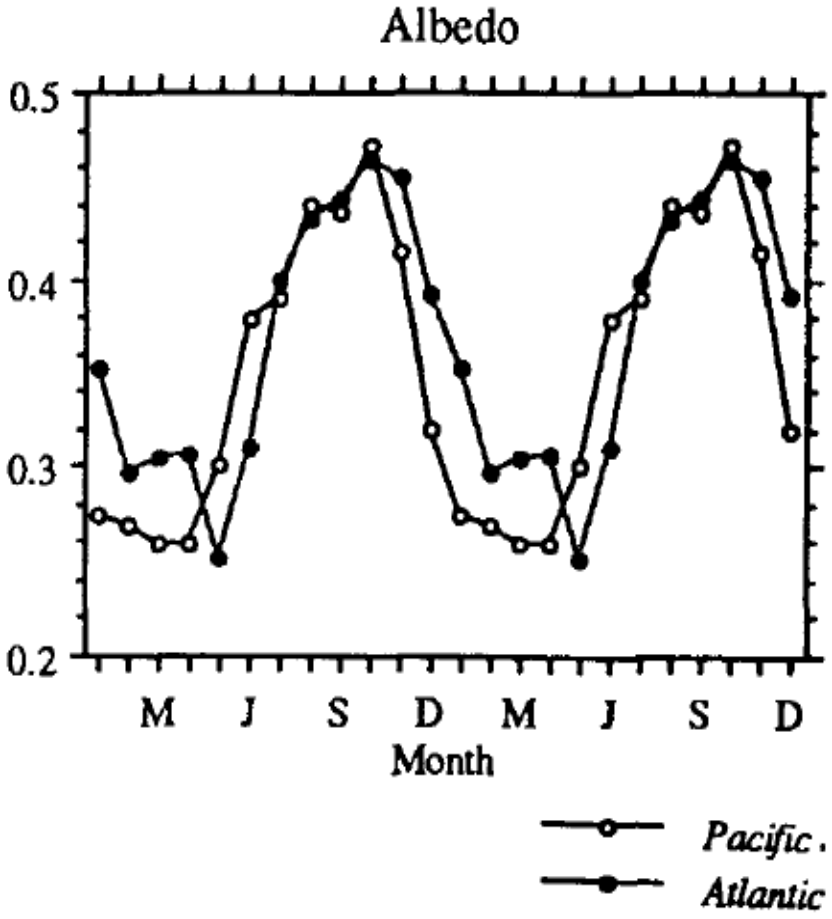

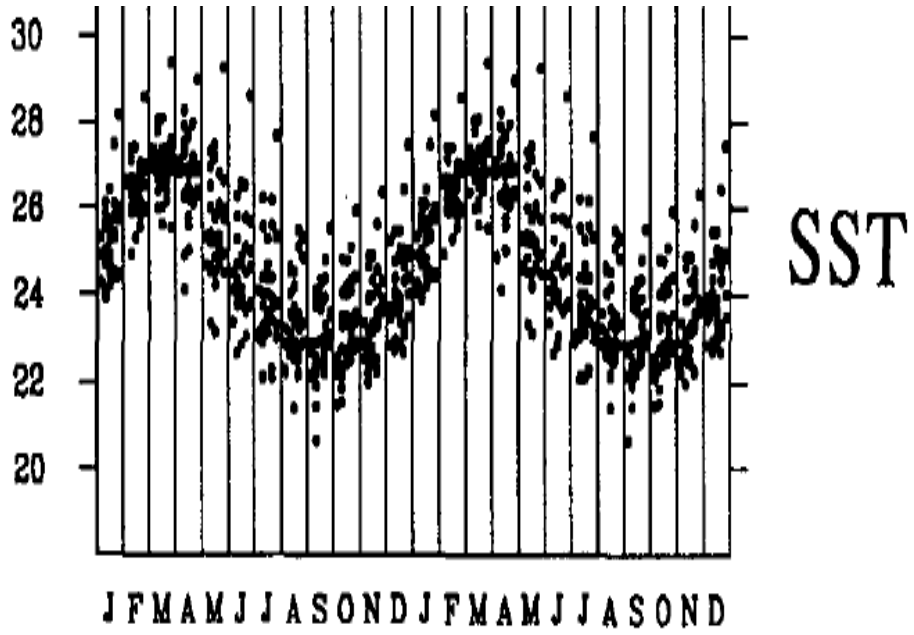

A negative correlation between low-level stratus cloud and SST

➔ A positive feedback between atmosphere and ocean!

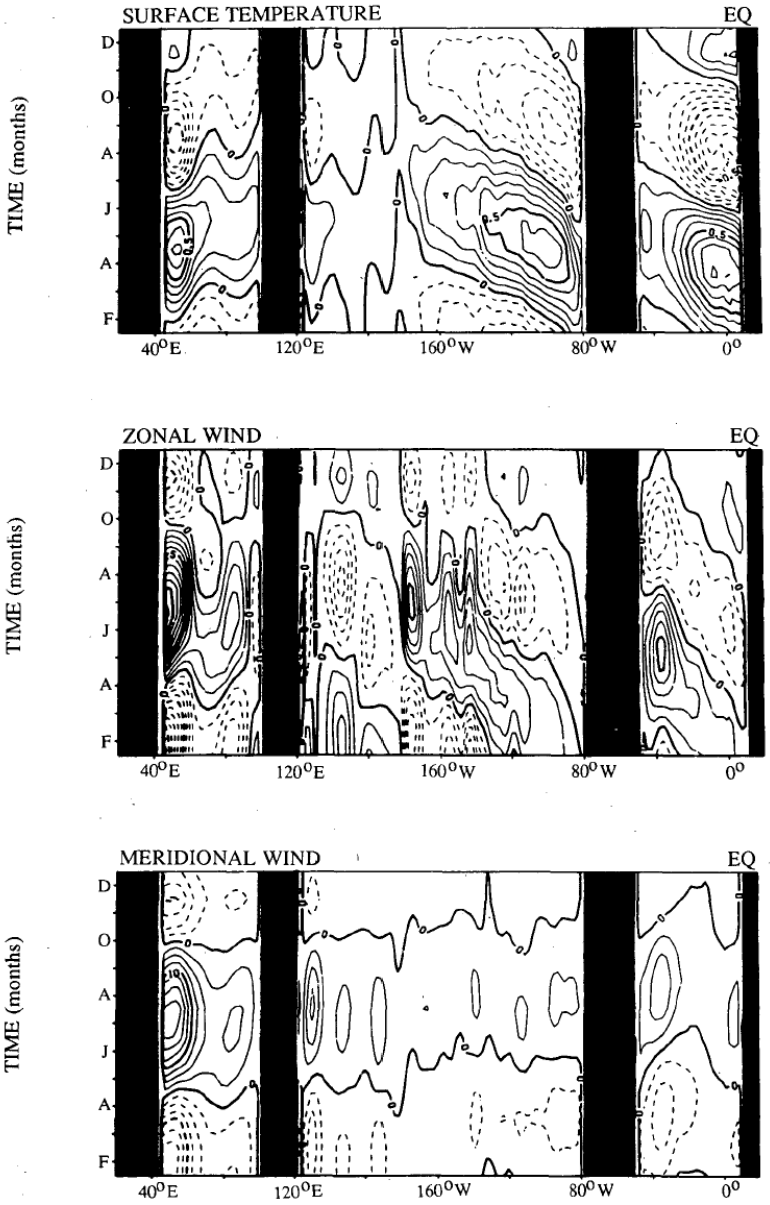

FIG. 15. Time–longitude plot of (a) the observed sea surface temperature, (b) the observed zonal component of surface winds, and (c) the observed meridional component of surface winds along the equator. Contour intervals are 0.5°C in (a) and 0.5 m s^{-1} in (b) and (c).

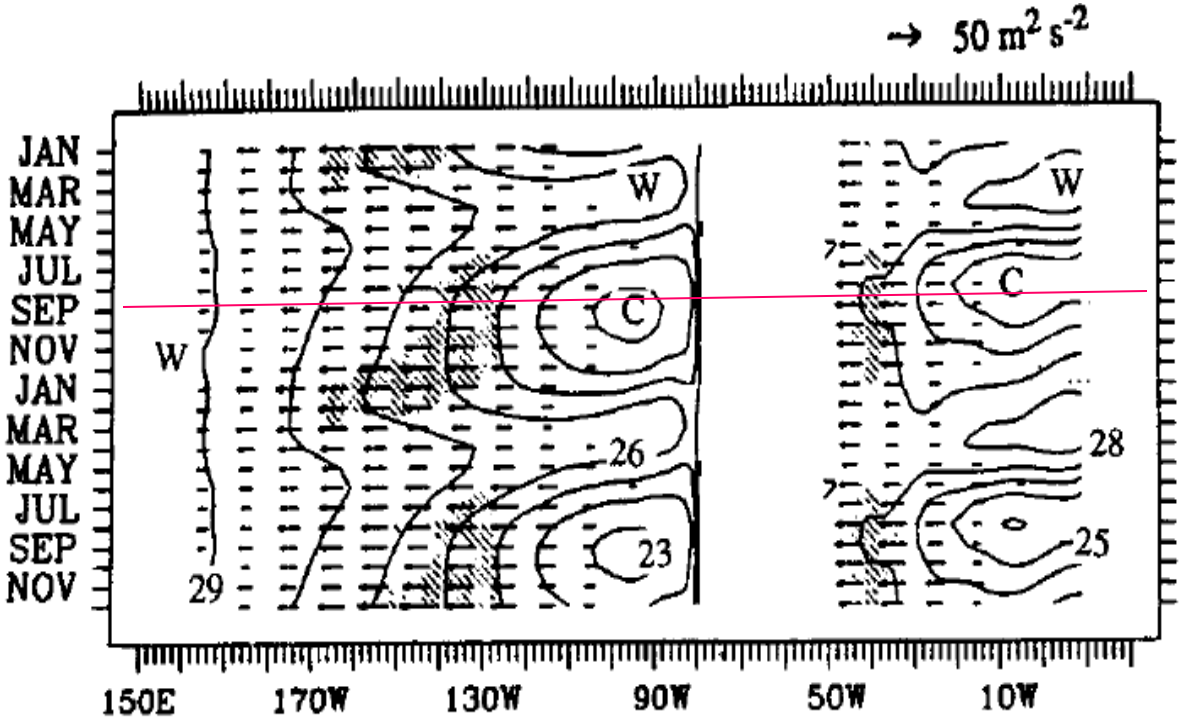

FIG. 12. Longitude–time section of equatorial (4°N–4°S) SST and zonal wind stress. The Pacific and Atlantic zonal wind-stress climatologies, which are plotted in a vector format, are taken for the years 1946–85 and 1951–75, respectively. The SST climatology, which is plotted as a contour field, is taken from the Sadler climatology (Sadler et al. 1987a,b). The SST contour interval is 1°C. Only zonal wind stresses > 10 $m^2 s^{-2}$ in magnitude are plotted, and the shading indicates zonal wind stresses > 40 $m^2 s^{-2}$.

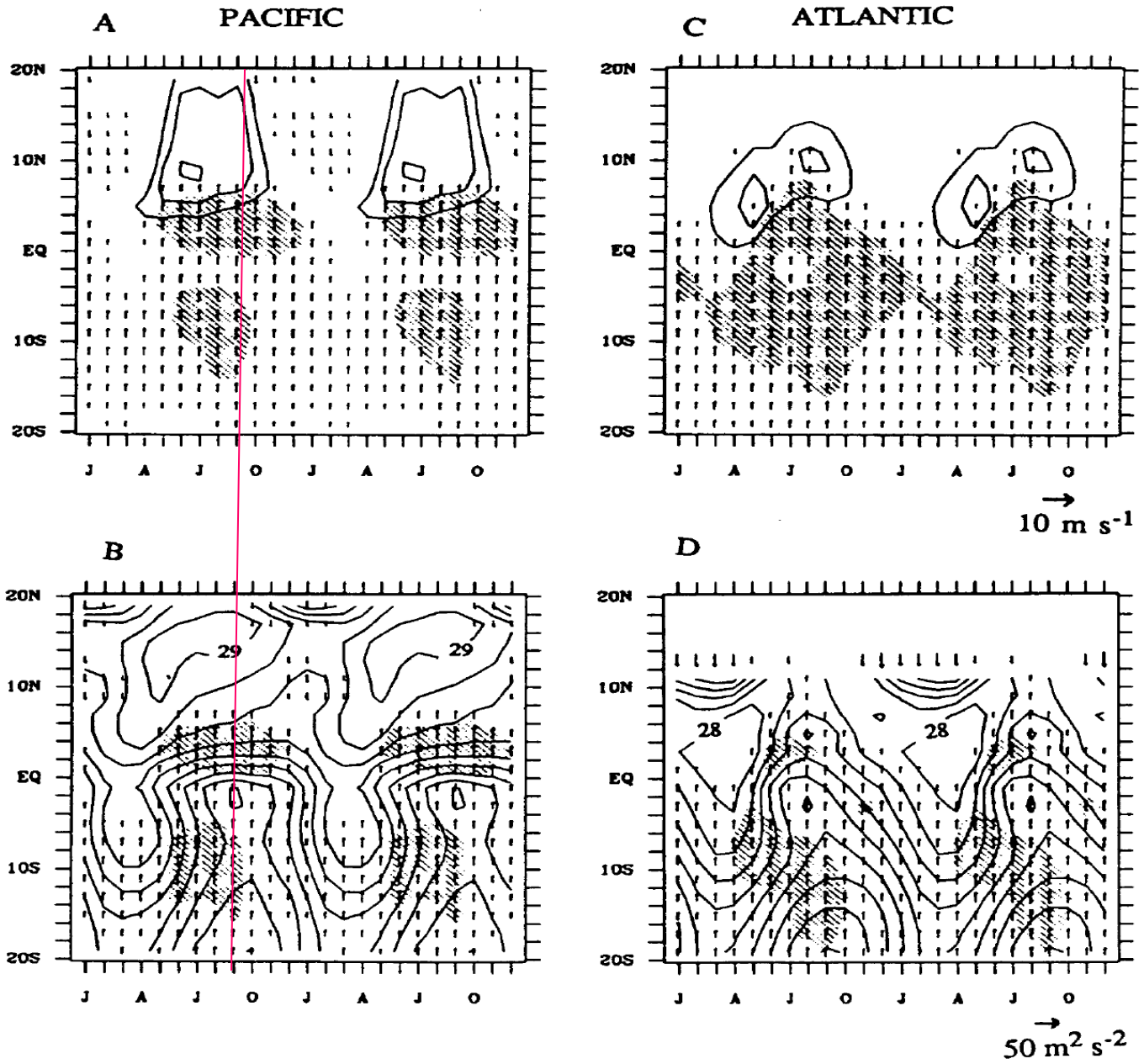

FIG. 13. Latitude–time sections of (a) OLR and the meridional component of the surface wind (in vector format) and (b) SST and meridional component of the wind stress (in vector format) for 104°–86°W. Here (c) and (d) are the same as (a) and (b), but for 16°W–4°E. In (a) and (c) only, OLR contours of 240, 225, 210 W m^{-2} and meridional winds > 2 m s^{-1} in magnitude are plotted, and the shading indicates meridional winds > 4 m s^{-1} in magnitude. In (b) and (d), the SST contour interval is 1°C. Only meridional stresses > 15 m^2 s^{-2} in magnitude are plotted, and the shading indicates meridional stresses > 30 m^2 s^{-2} in magnitude.

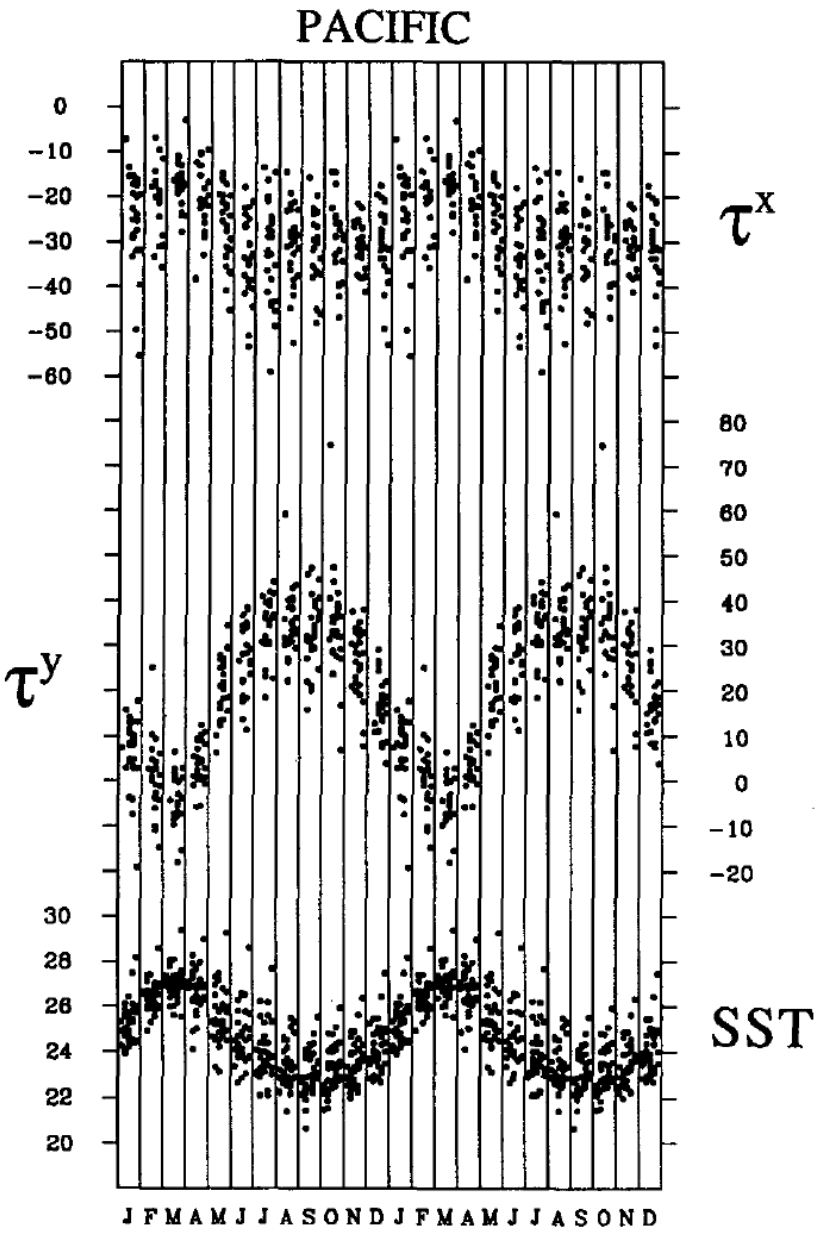

FIG. 14. As in Fig. 4 but for the zonal wind stress to the west (4°N–4°S, 130°–110°W), the meridional wind stress to the north (8°N–0°, 120°–100°W) of the Pacific cold tongue, and the cold tongue SST (4°N–4°S, 104°–86°W).

A more robust relationship between meridional wind stress and SST implies a possible dynamic air-sea feedback mechanism!

2. Theories

A Coupled Ocean–Atmosphere Instability of Relevance to the Seasonal Cycle

PING CHANG

Department of Oceanography, Texas A&M University, College Station, Texas

S. GEORGE PHILANDER

Atmospheric and Oceanic Science Program, Princeton University, Princeton, New Jersey

(Manuscript received 13 September 1993, in final form 11 May 1994)

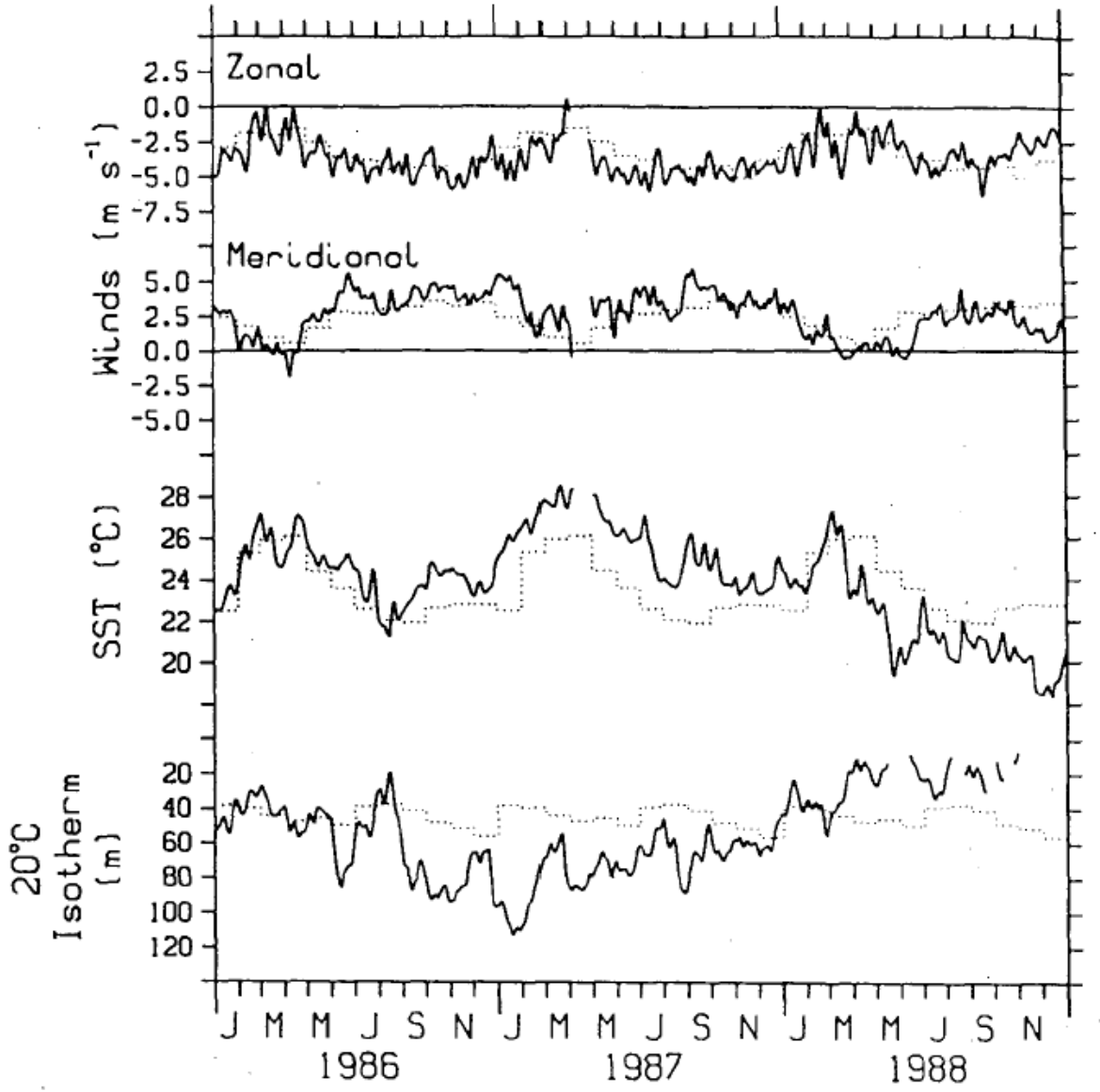

FIG. 1. Time series of zonal and meridional surface wind, SST, and depth of the 20°C isotherm at 0°, 110°W for the three years 1986–88. Solid lines are the measured values, and dotted lines are the monthly mean climatological values based on the historical data from the mooring at this location (from Hayes et al. 1991).

Lindzen-Nigam model

$$E\tau^x - f\tau^y = -\alpha\left(\frac{\partial\phi}{\partial x} - A\frac{\partial T}{\partial x}\right) \qquad (1)$$

$$E\tau^y + f\tau^x = -\alpha\left(\frac{\partial\phi}{\partial y} - A\frac{\partial T}{\partial y}\right) \qquad (2)$$

$$\phi + B\left(\frac{\partial\tau^x}{\partial x} + \frac{\partial\tau^y}{\partial y}\right) = 0, \qquad (3)$$

where τ^x and τ^y are the zonal and meridional component of the wind stress, ϕ is the geopotential at the top of the boundary layer, T is the sea surface temperature (SST), and E is a mechanical damping due to vertical diffusion of momentum and surface drag. $A = gH_0/2T_0$ and $B = gH_0/\mu\alpha$ measure the strength of the pressure force induced by the SST gradients and the strength of the "back pressure" effect; H_0 is the depth of the boundary layer; T_0 is a reference temperature; μ is an inverse relaxation time for the adjustment of the boundary layer height; and α converts the wind speeds into surface wind stresses. In the LN model, it is assumed

Cane-Zebiak model

$$T_t + \bar{u}_1 T_x + \bar{v}_1 T_y + \frac{\bar{w}}{H_1}(T - \gamma h) + u_1 \bar{T}_x + v_1 \bar{T}_y + w \bar{T}_z + \epsilon T - \kappa \nabla^2 T = 0 \quad (4)$$

$$\begin{bmatrix} u_1 \\ v_1 \end{bmatrix} = \frac{H_2}{H} \begin{bmatrix} u_e \\ v_e \end{bmatrix}, \quad w = \frac{H_1 H_2}{H} \nabla \cdot \mathbf{v}_e \quad (5)$$

$$\begin{bmatrix} u_e \\ v_e \end{bmatrix} = \frac{1}{\Delta_0} \begin{bmatrix} r_s \tau^x + f \tau^y \\ r_s \tau^y - f \tau^x \end{bmatrix}, \quad \Delta_0 = H_1 (r_s^2 + f^2), \quad (6)$$

where H_1 and H are the depth of the mixed layer and the mean depth of the thermocline; H_2 is defined as the difference between H and H_1; $\bar{u}_1$, $\bar{v}_1$ and u_1, v_1 represent the zonal and meridional component of the mean and

a. The coupled unstable modes at the long-wave limit

In the long-wave limit, $k = 0$; if it is of the form $\tau^y = \tau(y)e^{\sigma t}$, Eqs. (1)–(4) can be reduced, by assuming $\gamma = \bar{T}_x = 0$, to a single eigenequation for the meridional wind stress τ:

$$\kappa \frac{d^2}{dy^2} D(\tau) - \frac{d}{dy}[\bar{v}_1 D(\tau)] - \left(\frac{\bar{W}}{H_1} + \epsilon\right) D(\tau) - \frac{H_2}{EHH_1} \frac{d}{dy}\left[\bar{T}_y \frac{\Delta}{\Delta_0} \tau\right] - \frac{H_2}{EH} \frac{d^2}{dy^2}\left[\bar{T}_z \frac{\Delta}{\Delta_0} \tau\right] = \sigma D(\tau), \quad (7)$$

where

$$D(\tau) = -\frac{B}{A} \frac{d^2\tau}{dy^2} + \frac{\Delta_a \tau}{H_1 E \alpha A},$$

$$\Delta = H_1(r_s E - f^2), \quad \Delta_a = H_1(E^2 + f^2).$$

The boundary conditions for the governing eigenvalue problem are

$$\tau = \frac{d\tau}{dy} = 0 \quad \text{as} \quad y \to \pm\infty. \quad (8)$$

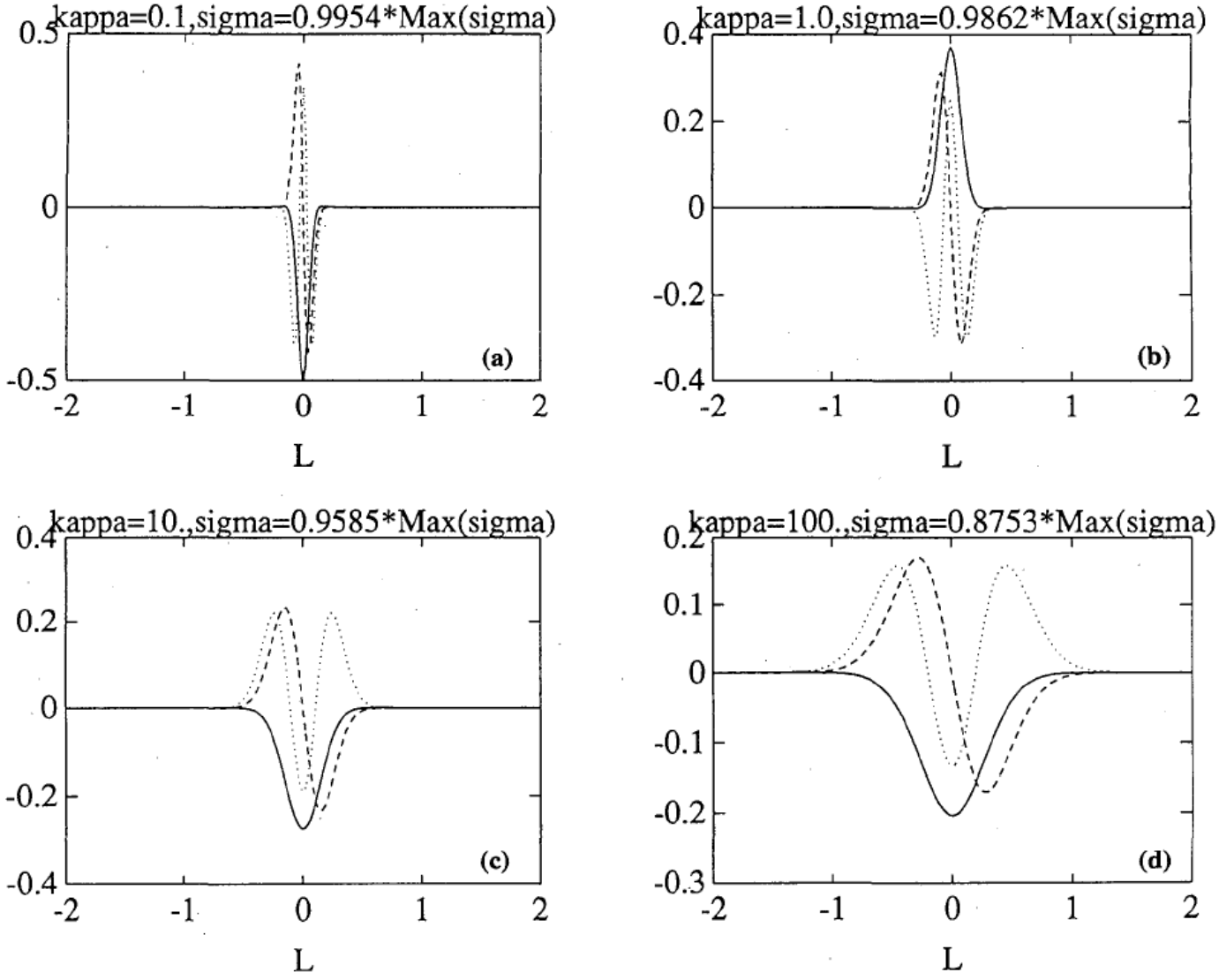

FIG. 4. Meridional structure τ^{ν} of the first three most unstable modes for (a) $\kappa = 0.1$ m^2 s^{-1}, (b) $\kappa = 1.0$ m^2 s^{-1}, (c) $\kappa = 10.0$ m^2 s^{-1}, and (d) $\kappa = 100.0$ m^2 s^{-1}. The corresponding maximum growth rates are $0.9954\sigma_0$ in (a), $0.9862\sigma_0$ in (b), $0.9585\sigma_0$ in (c), and $0.8753\sigma_0$ in (d), where σ_0 is the maximum growth rate in the absence of diffusion.

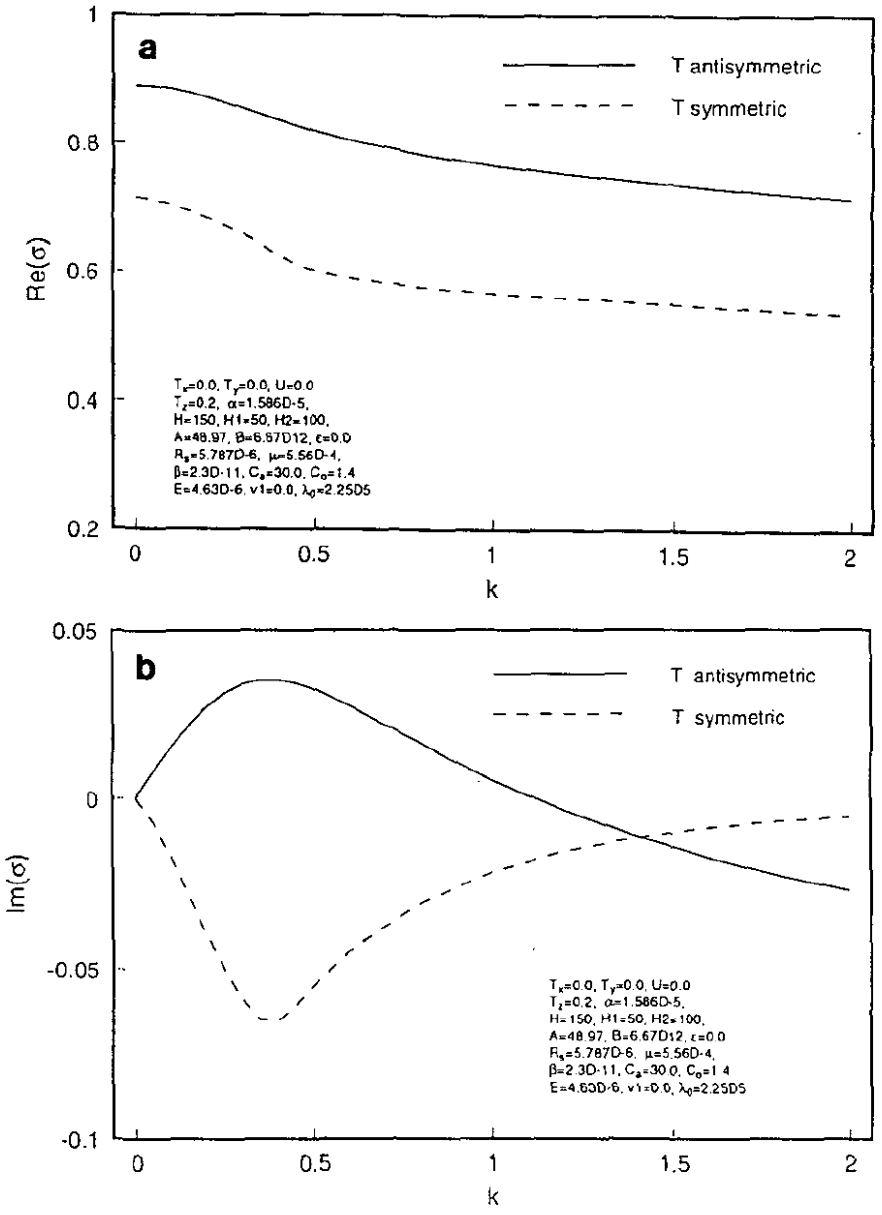

FIG. 5. Dispersion diagram of the most unstable coupled antisymmetric and symmetric SST modes in the absence of mean background fields: (a) the growth rate $\mathrm{Re}(\sigma)$ of the antisymmetric SST mode (solid line) and the symmetric SST mode (dashed line); (b) the frequency $\mathrm{Im}(\sigma)$ of the antisymmetric SST mode (solid line) and the symmetric SST mode (dashed line). In the figures $\mathrm{Re}(\sigma)$ and $\mathrm{Im}(\sigma)$ are nondimensionalized by $\max(\sigma) = \mu\alpha H_2 \bar{T}_z/(2T_0 H r_s)$, and k is nondimensionalized by $L^{-1} = \beta/\sqrt{E r_s}$.

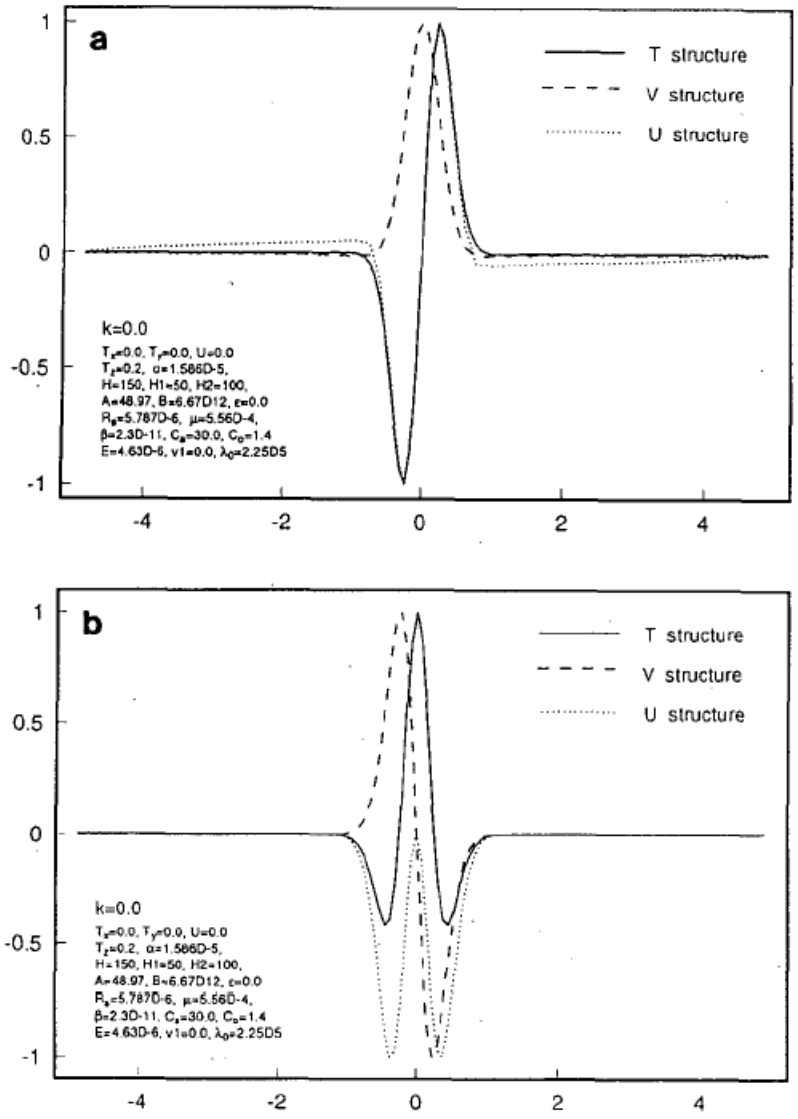

FIG. 6. Structure of (a) the antisymmetric SST mode and (b) the symmetric SST mode at $k = 0$. In the figures, SST is plotted by solid line, and the zonal and meridional components of wind are plotted by dotted and dashed lines, respectively. The x axis is measured by the frictional scale $L = \sqrt{Er_s/\beta}$.

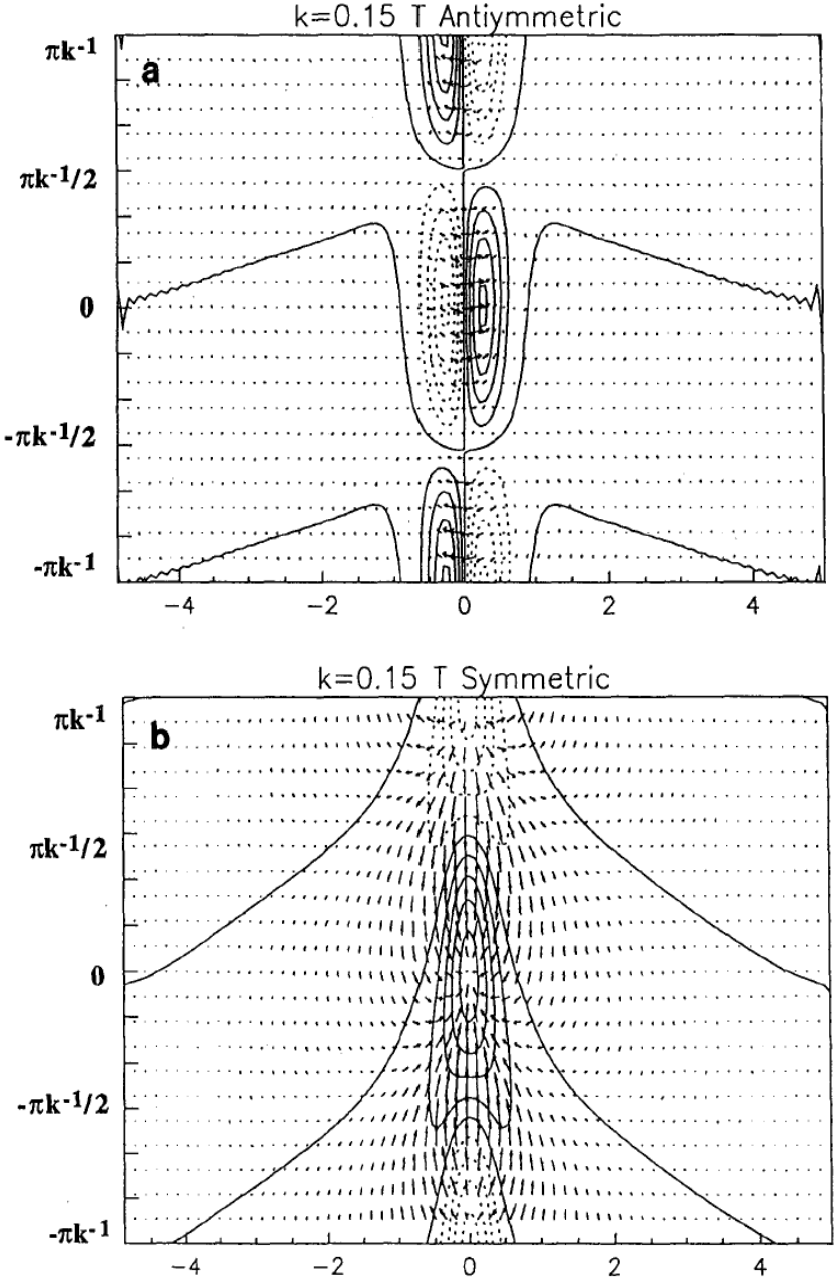

FIG. 8. Structure of SST (contour) and wind stresses (vector) for (a) the most unstable antisymmetric SST mode and (b) the most unstable symmetric SST mode at $k = 0.15$ (the corresponding wavelength and period are about 9500 km and one year, respectively). The x axis is measured by the frictional scale $L = \sqrt{Er_s/\beta}$.

Schematic diagram illustrating a positive feedback Between the atmosphere and ocean by Chang and Philander (1994)

Meridional wind-upwelling-SST feedback

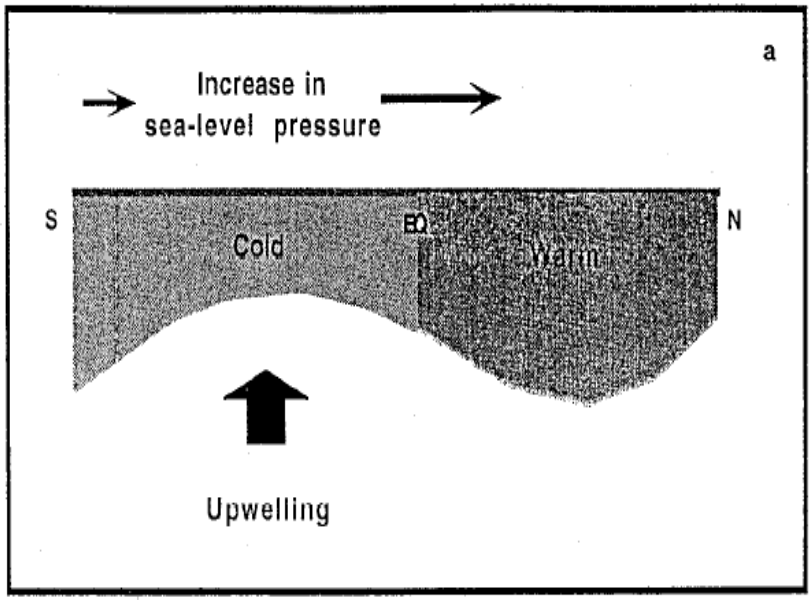

Tellus (1994), 46A, 340–350
Printed in Belgium – all rights reserved

Copyright © Munksgaard, 1994
TELLUS
ISSN 0280–6495

A coupled ocean-atmosphere model of relevance to the ITCZ in the eastern Pacific

By SHANG-PING XIE[1]* and S. GEORGE H. PHILANDER, *Program in Atmospheric and Oceanic Sciences, Princeton University, Princeton, NJ 08544-0710, USA*

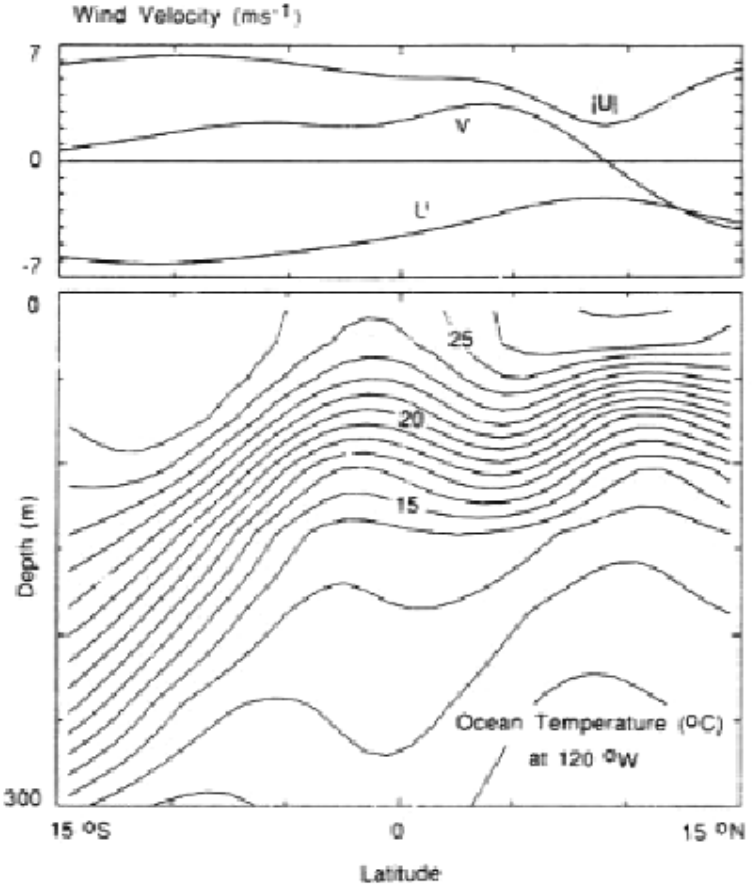

Fig. 1. Meridional section of annual-mean ocean temperature (from Levitus (1982) data set), and distribution of surface wind velocity (from Comprehensive Ocean-Atmospheric Data Set) along 120° W. The center of the ITCZ is where meridional wind vanishes.

2.1. Model atmosphere

The model atmosphere is described by the equations

$$AU' - fV = 0, \tag{2.1}$$

$$AV + fU' = -\Phi_x, \tag{2.2}$$

$$A\Phi + C_a^2 V_y = -Q_a, \tag{2.3}$$

where (U', V) are the surface wind components, Φ is the geopotential difference between the ground and tropopause, A is the damping rate, f is the Coriolis parameter and C_a is the long gravity wave speed. Matsuno (1966) and Gill (1980) used such a model to study the atmospheric response to prescribed heating. Latent heat release in our model, Q_a, depends on sea surface temperature T in the following manner,

$$Q_a = K_Q(T - T_c)\, H(T - T_c), \tag{2.4}$$

where H is Heaviside's step function

$$H(x) = \begin{cases} 1, & \text{if} \quad x \geqslant 0, \\ 0, & \text{otherwise.} \end{cases} \tag{2.5}$$

2.2. Model ocean

The motion of the upper ocean above the thermocline is assumed to be governed by the linear 1.5-layer reduced-gravity model equations,

$$(hu)_t - f(hv) = \tau_x/\rho - a(hu) + \nu(hu)_{yy}, \tag{2.7}$$

$$(hv)_t + f(hu) = -c^2 h_y + \tau_y/\rho - a(hv) + \nu(hv)_{yy}, \tag{2.8}$$

$$h_t + (hv)_y = -a(h - H), \tag{2.9}$$

where h, the depth of the thermocline, has an equilibrium value $H = 100$ m, hu is the mass transport from the surface to h, $c = (g'H)^{1/2}$ is the phase speed of long gravity wave with g' denoting the reduced gravity, ρ is the water density, a is the damping rate* and ν is the eddy viscosity coefficient. Nonlinear model calculations show that the meridional momentum advection terms are negligible. A linearized bulk formula is used to obtain the wind stress

$$(\tau_x, \tau_y) = C_D^*(U, V), \tag{2.10}$$

where, $C_D^* = \rho_a C_D U_0$ with ρ_a, C_D and U_0 being air density, drag coefficient and mean surface wind

the thermocline. For simplicity, we use h as the depth of mixed layer. Then the temperature in the mixed layer, which is also the SST, can be obtained by solving the equation

$$\frac{\partial T}{\partial t}+v\frac{\partial T}{\partial y}=\frac{1}{h}\left(\frac{Q}{\rho c_p}-W_e\,\Delta T\right)+\kappa\frac{\partial^2 T}{\partial y^2}. \tag{2.11}$$

The rate for upper thermocline water to be entrained into the mixed layer is calculated using Kraus–Turner's formula (Kraus and Turner, 1967; Niiler and Kraus, 1977),

$$W_e\,\Delta T=\begin{cases}\dfrac{1}{h(1-m_e\mathrm{Ri}^{-1})}\left(\dfrac{2mu_*^3}{\alpha g}-h\dfrac{Q}{\rho c_p}\right) \\ \qquad \text{if} \quad W_e>0, \\ 0, \qquad \text{otherwise,}\end{cases} \tag{2.12}$$

where Ri is the Richardson number

$$\mathrm{Ri}=\frac{\alpha g\,\Delta T h}{|\Delta u|^2}. \tag{2.13}$$

u_* is proportional to the wind speed, i.e.,

$$u_*=\left(\frac{\tau}{\rho}\right)^{1/2}=\left(\frac{\rho_a}{\rho}C_D\right)^{1/2}|U|. \tag{2.14}$$

simulate the undercurrent, we simply specify the vertical shear in (2.12) as a time-invariant function that decays away from the equator,

$$\frac{m_c}{R_i} h = \frac{m_c}{\alpha g \Delta T} |\Delta u|^2$$

$$= h_* \exp\left[-\frac{1}{2}\left(\frac{y}{R}\right)^2 \right]. \tag{2.15}$$

The surface heat flux may be written as:

$$Q = Q_0 - L\rho_* C_E (1 - \mathrm{RH}) |U| q_s(T)$$

$$= Q_0 - C_E^* |U| q_s(T), \tag{2.16}$$

tropics. The saturated moisture content q_s is given by the Clausius–Clapeyron equation

$$q_s(T) = q_0 \exp\left[\frac{L}{R_*}\left(\frac{1}{T_0} - \frac{1}{T}\right)\right], \tag{2.17}$$

$$Q_0 = C_E^* U_{\min} q_s(T^*), \tag{2.18}$$

$$T^* = T_c + \frac{(T_p - T_c)}{L_y^2} y^2 \tag{2.19}$$

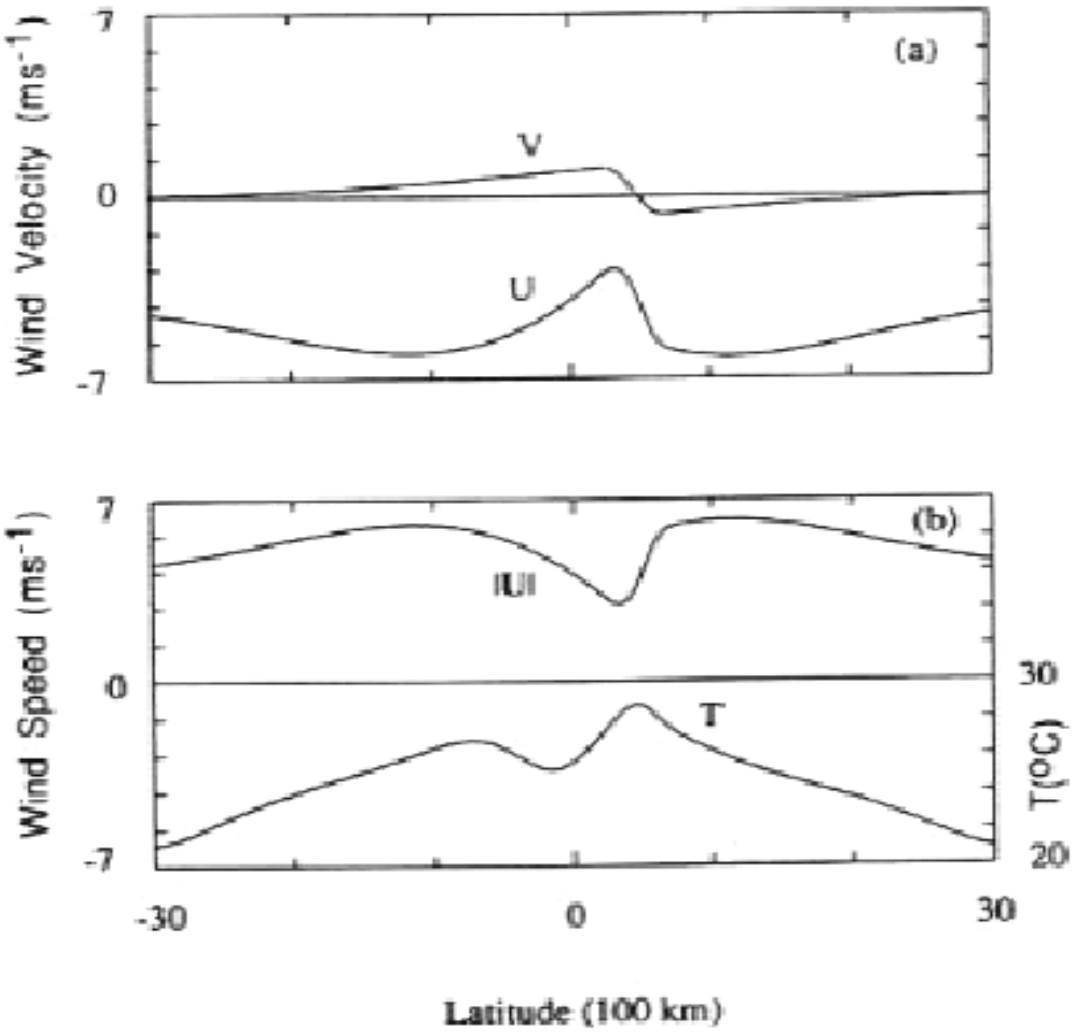

Fig. 5. Meridional distributions of (a) zonal and meridional wind velocities, and (b) wind speed and SST, in an asymmetric solution to the slab mixed-layer model where the depth of the thermocline is fixed as a constant.

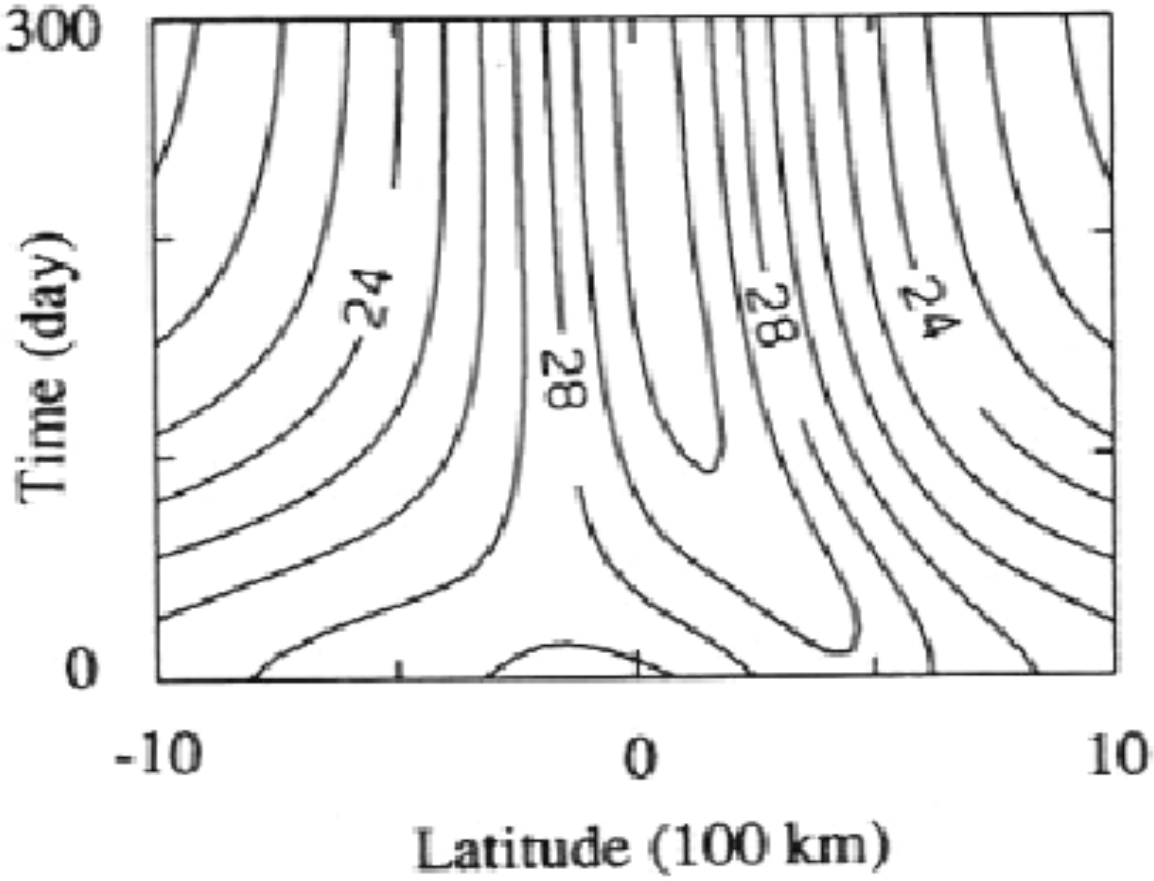

Fig. 6. Latitude-time section of SST in a case with zero equatorial upwelling. The initial condition is the equatorially asymmetric state shown in Fig. 5.

Schematic diagram illustrating a positive feedback between the atmosphere and ocean by Xie and Philander (1994)

Wind-evaporation-SST feedback

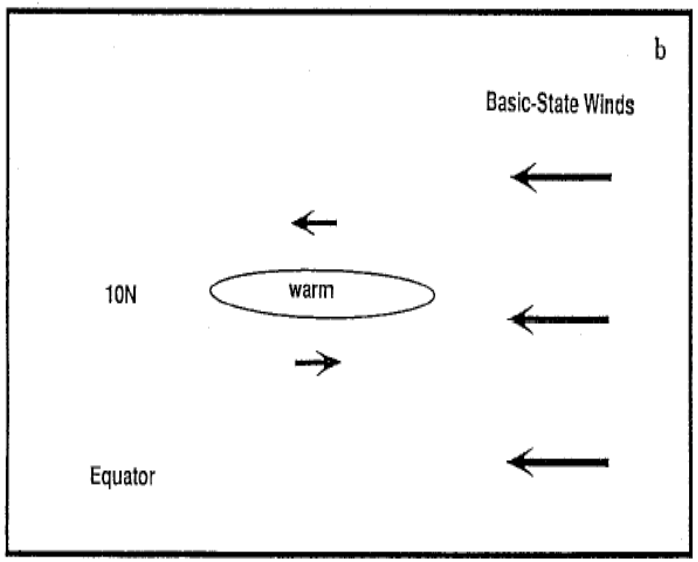

Air–Sea Interactions of Relevance to the ITCZ: Analysis of Coupled Instabilities and Experiments in a Hybrid Coupled GCM

TIANMING LI

University Corporation for Atmospheric Research, Visiting Scientist Program, Naval Research Laboratory, Monterey, California

(Manuscript received 30 October 1995, in final form 24 June 1996)

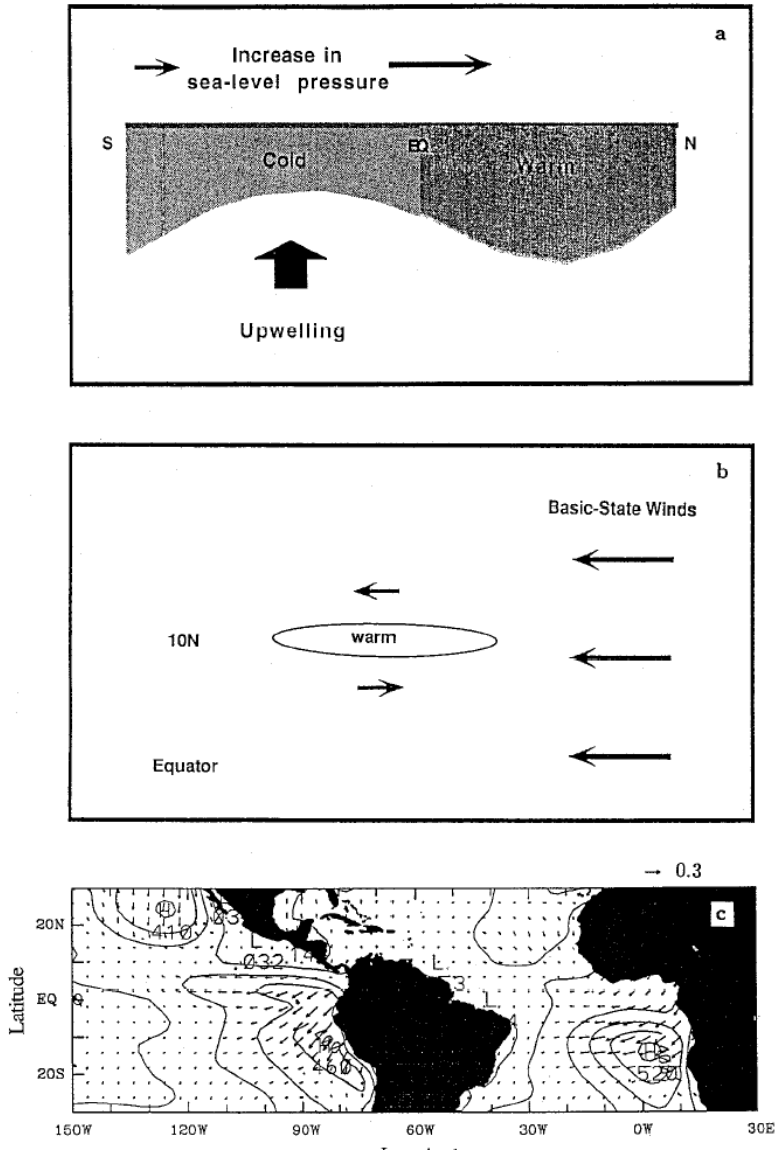

FIG. 1. Schematic diagrams showing (a) the coupled ocean–atmosphere instability of the first kind, the positive feedback between the meridional wind and SST, proposed by Mitchell and Wallace (1992) and Chang and Philander (1994), and (b) the coupled ocean–atmosphere instability of the second kind, the evaporation–wind feedback (Xie and Philander 1994). (c) ISCCP monthly mean stratus cloud fields. Contours represent the annual mean field and vectors represent annual harmonics (upward denotes a maximum amplitude in January, rightward in April, and so on).

The governing equations of the 2½-layer model

$$\frac{\partial U_{\mathrm{L}}}{\partial t} - \beta y V_{\mathrm{L}} = -\epsilon U_{\mathrm{L}}, \tag{2.1}$$

$$\frac{\partial V_{\mathrm{L}}}{\partial t} + \beta y U_{\mathrm{L}} = -\frac{\partial \phi}{\partial y} - \epsilon V_{\mathrm{L}}, \tag{2.2}$$

$$\begin{aligned}\frac{\partial \phi}{\partial t} + C_0^2(1-\delta I)\frac{\partial V_{\mathrm{L}}}{\partial y} = {} & C_0^2 d(\delta B - 1)\frac{\partial V_{\mathrm{B}}}{\partial y} \\ & - G(T_s - T_0) \\ & - \delta F|\mathbf{V}_s|(q_s - q_0) - \epsilon\phi,\end{aligned} \tag{2.3}$$

$$E U_{\mathrm{B}} - \beta y V_{\mathrm{B}} = 0, \tag{2.4}$$

$$E V_{\mathrm{B}} + \beta y U_{\mathrm{B}} = -\frac{\partial \phi}{\partial y} + A\frac{\partial T_s}{\partial y}, \tag{2.5}$$

$$P_r = \delta M = \delta b\left[E_v - \frac{1}{g}\int_{pu}^{ps} \nabla\cdot(\bar{q}\mathbf{V})\, dp\right], \tag{2.6}$$

where

$$E_v = \rho_a C_D|\mathbf{V}_s|(q_s(T_s) - q_0) \tag{2.7}$$

b. The oceanic model

$$\frac{\partial u_m}{\partial t} - \beta y v_m = \frac{\tau^x}{\rho H} - r u_m, \tag{2.9}$$

$$\frac{\partial v_m}{\partial t} + \beta y u_m = -g' \frac{\partial h}{\partial y} + \frac{\tau^y}{\rho H} - r v_m, \tag{2.10}$$

$$\frac{\partial h}{\partial t} + H \frac{\partial v_m}{\partial y} = -rh, \tag{2.11}$$

$$r_s u_s - \beta y v_s = \frac{\tau^x}{\rho H_1}, \tag{2.12}$$

$$r_s v_s + \beta y u_s = \frac{\tau^y}{\rho H_1}, \tag{2.13}$$

$$\begin{aligned} \frac{\partial T}{\partial t} = & -v \bar{T}_y - \bar{v} T_y \\ & - [M(\bar{w} + w) - M(\bar{w})] \bar{T}_z \\ & - M(\bar{w}) T_z + \frac{Q}{\rho C_w H_1}, \end{aligned} \tag{2.14}$$

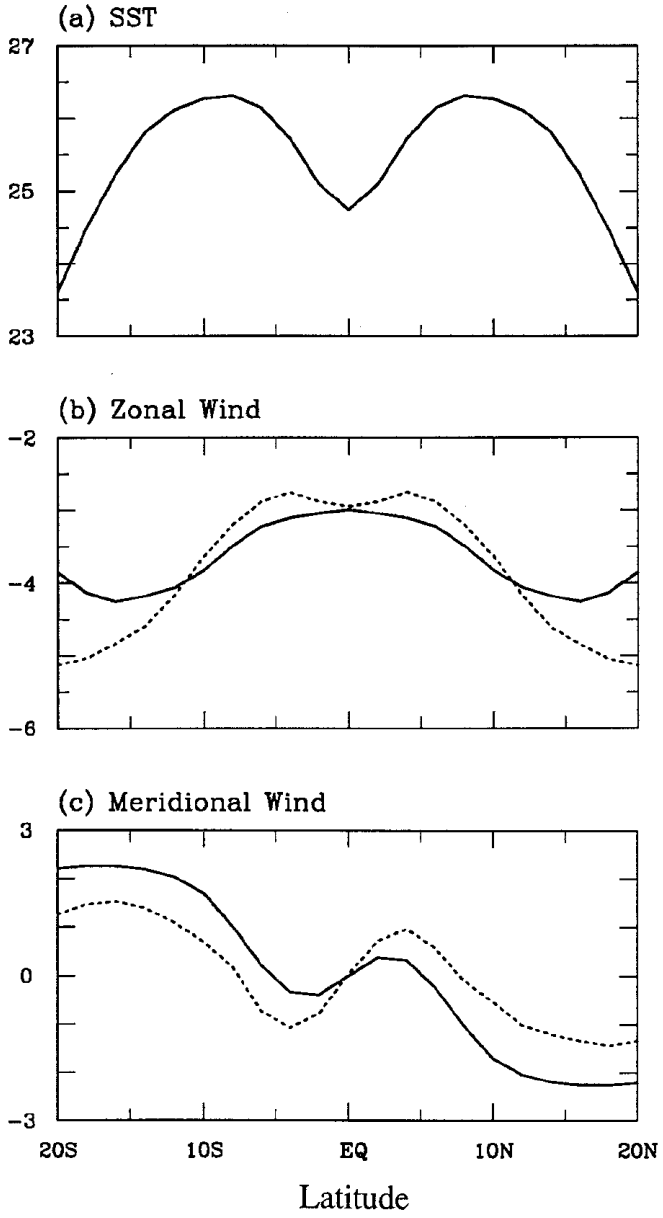

FIG. 2. The solid lines show the symmetric component of the observed annual mean (a) SST (°C), (b) zonal wind, and (c) meridional wind component (m s^{-1}) in the eastern Pacific (averaged between 140°W and 80°W). The dashed lines in (b) and (c) show the model-simulated wind components forced by SST in (a).

The model atmosphere and ocean are coupled once per day. For simplicity a linearized wind stress formula is adopted, which has the form

$$\boldsymbol{\tau} = \rho_a C_D V_0 \, \mathbf{V}'_s, \tag{2.15}$$

where $V_0 = 5$ m s^{-1} represents a constant surface wind speed and $\mathbf{V}'_s$ denotes anomalous surface wind. The evaporation anomaly at the ocean surface can be written as

$$Q_{LH} = \rho_a C_D L_c[|\mathbf{V}'_s + \bar{\mathbf{V}}_s|(q_s - q_a) - |\bar{\mathbf{V}}_s|(\bar{q}_s - \bar{q}_a)], \tag{2.16}$$

where $\bar{\mathbf{V}}_s$ stands for the basic-state wind field; q_s and q_a are calculated from total sea surface temperature; $\bar{q}_s$ and $\bar{q}_a$ are computed from the basic-state SST; and $L_c = 2.5 \times 10^6$ J kg^{-1} represents latent heat of vaporization per unit mass.

Following Li and Philander (1996), an empirical formula is used to determine low-level marine stratus clouds. The shortwave radiation anomaly at the ocean surface can be expressed as

$$Q_{\mathrm{SW}} = [Q_0(1 - 0.62C) - Q_0(1 - 0.62\bar{C})] \times (1 - \lambda), \tag{2.17}$$

The initial condition is an antisymmetric SST perturbation that has the form

$$T = \hat{T}\frac{y}{L}\exp\left(-\frac{y^2}{2L^2}\right), \tag{2.18}$$

where $L = 10^\circ$ in latitude and $\hat{T} = 0.5\exp(0.5)$. This perturbation has a maximum amplitude at $y = L$ and a minimum at $y = -L$. All other variables are set to be zero initially.

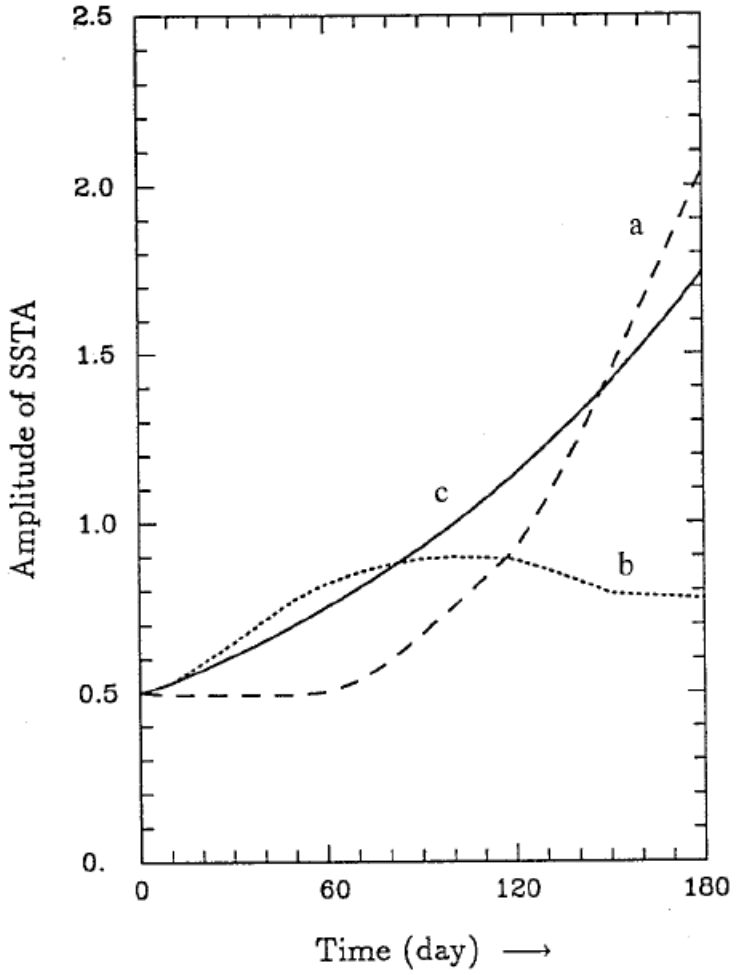

FIG. 3. The time evolution of amplitude of the SST anomaly (°C) in the presence of (a) the meridional wind–SST feedback (dashed line), (b) the evaporation–wind feedback (dotted line), and (c) the low-level stratus cloud–SST feedback (solid line) mechanisms.

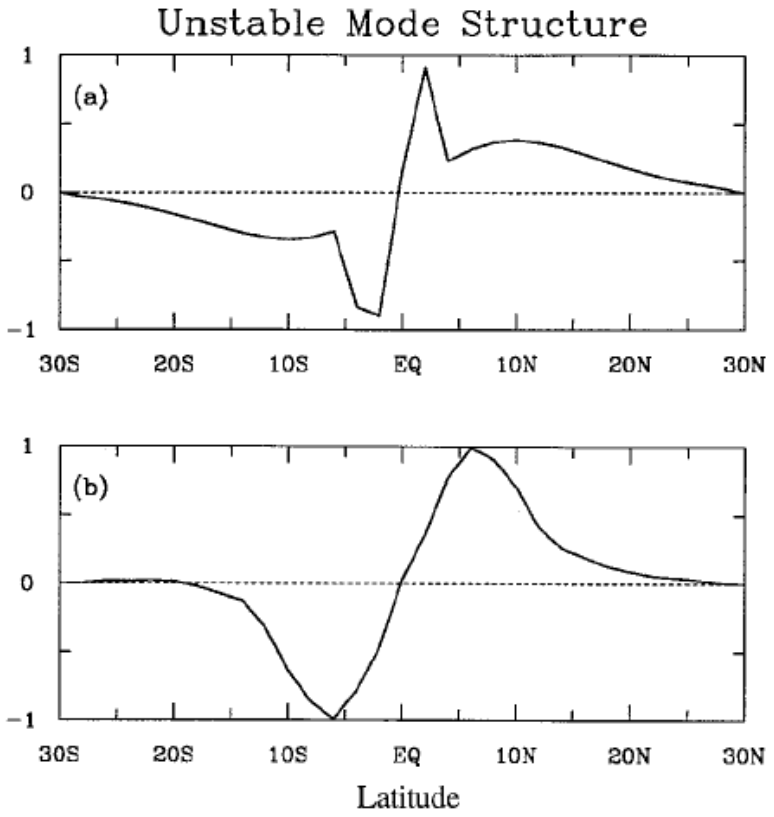

FIG. 4. The meridional structure of unstable SST modes in the presence of (a) the meridional wind–SST feedback (at day 180) and (b) the evaporation–wind feedback (at day 60). The SSTs have been normalized in terms of their maximum values so that the amplitudes are a unit.

evaporation–wind feedback, one can readily derive the growth rate from (2.14) and (2.17), which is

$$\text{growth rate} = \frac{Q_0 0.62 \alpha_1 (1 - \lambda)}{\rho C_w H_1}. \qquad (2.25)$$

Equation (2.25) states that the growth rate depends on the cloud–SST feedback coefficient α_1, on the mixed layer depth H_1, and on the solar radiation at the top of the atmosphere Q_0. For given annual-mean insolation at

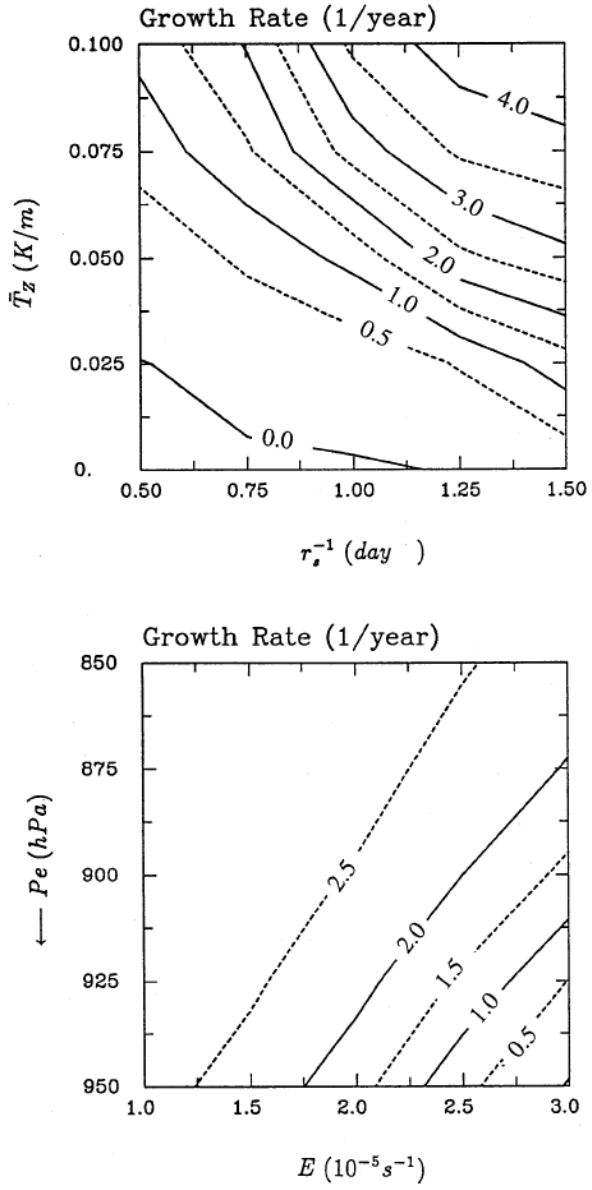

FIG. 5. Growth rates (yr^{-1}) as a function of (a) the basic-state vertical temperature gradient and friction coefficient in the ocean mixed layer and (b) the pressure at the top of the atmospheric boundary layer and the Ekman number in the presence of the meridional wind–SST feedback.

One important question related to the evaporation–wind feedback is why it leads to an instability. We first consider a linear version of (2.1)–(2.16). Linearized by a uniform basic state for both the SST and the zonal wind components, the governing equation for a steady-state atmosphere in a constant f plane can be written as

$$\epsilon U_{\mathrm{L}} - fV_{\mathrm{L}} = 0, \tag{2.19}$$

$$\epsilon V_{\mathrm{L}} + fU_{\mathrm{L}} = -\frac{\partial \phi}{\partial y}, \tag{2.20}$$

$$\epsilon\phi + C_0^2(1 - \bar{I})\frac{\partial V_L}{\partial y} = C_0^2 d(\bar{B} - 1)\frac{\partial V_{\mathrm{B}}}{\partial y} - GT - KU_{\mathrm{B}}, \tag{2.21}$$

$$EU_{\mathrm{B}} - fV_{\mathrm{B}} = 0, \tag{2.22}$$

$$EV_{\mathrm{B}} + fU_{\mathrm{B}} = -\frac{\partial \phi}{\partial y} + A\frac{\partial T}{\partial y}, \tag{2.23}$$

$$\frac{\partial T}{\partial t} = -\frac{\rho_a C_D L_c \Delta q \bar{U}}{\rho C_w H_1 |\bar{U}|} U_{\mathrm{B}}, \tag{2.24}$$

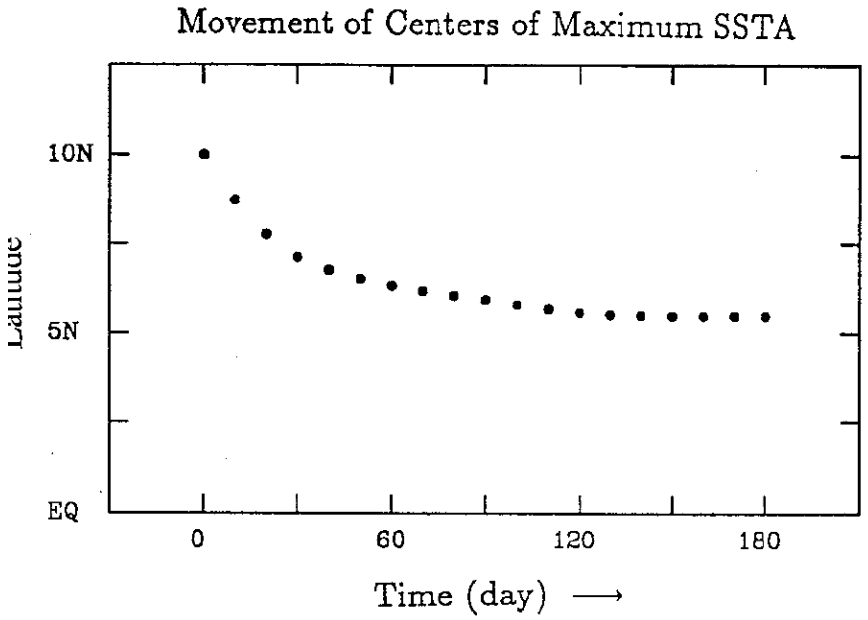

FIG. 6. The meridional movement of maximum SST anomalies in ıe presence of the evaporation–wind feedback mechanism. Initially, ıe SST perturbation is at 10°N.

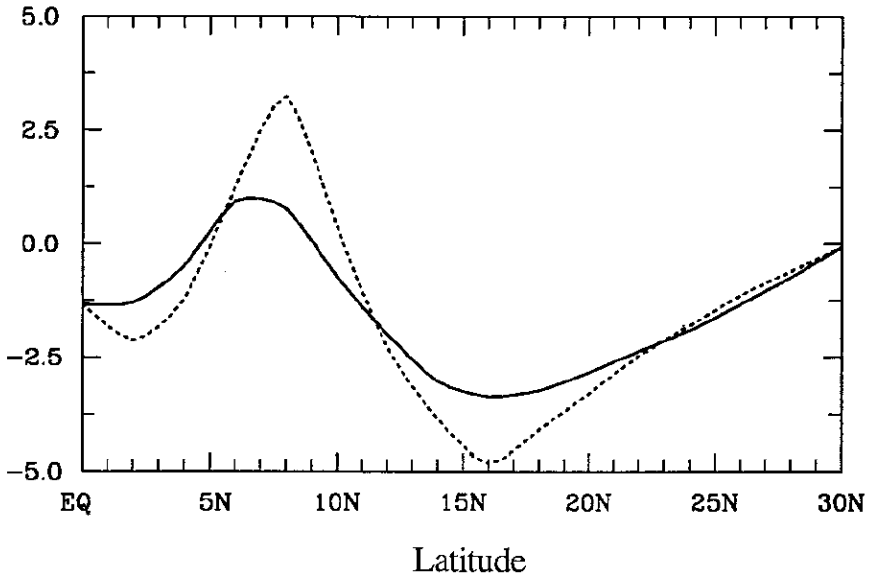

FIG. 7. The time tendency for SST (units: 10^{-8} K s^{-1}) at $t = 0$ in the cases of linear (solid line) and nonlinear (dotted line) atmospheric heating, in the presence of the evaporation–wind feedback.

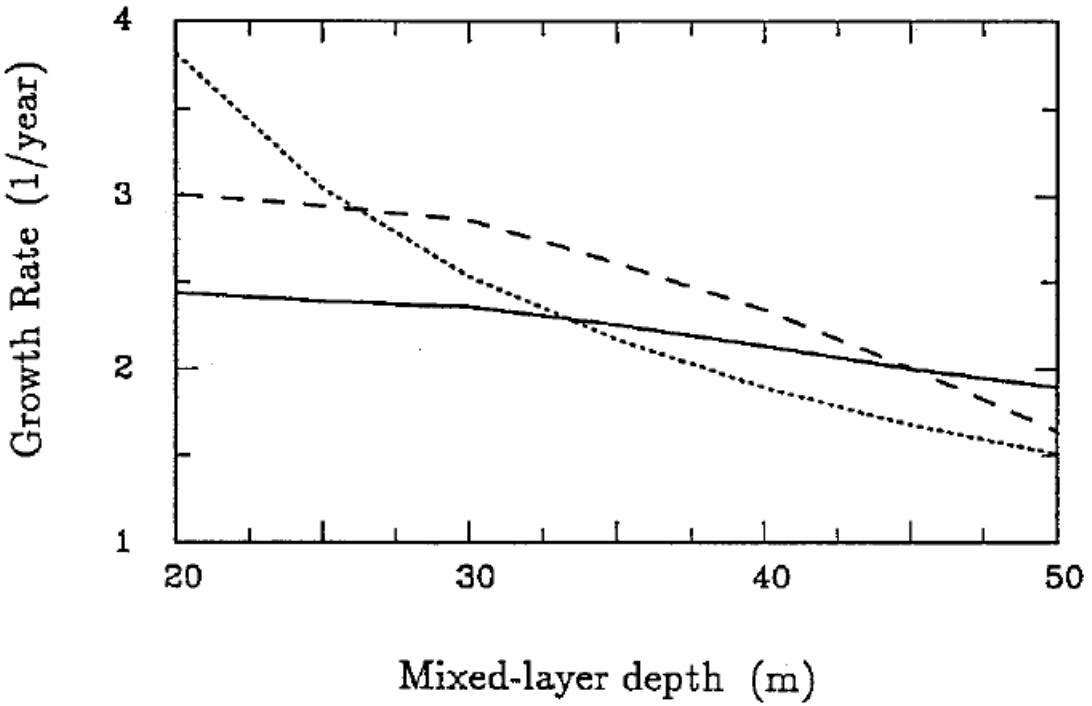

FIG. 8. Growth rates (yr^{-1}) as a function of the oceanic mixed-layer depth in the presence of the meridional wind–SST feedback (dashed line), the evaporation–wind feedback (solid line), and the stratus cloud–SST feedback (dotted line) mechanisms.

Li 1997, JAS

Theoretical studies above indicate that three types of ocean-atmosphere interactions can favor the occurrence of an anti-symmetric SST-wind pattern relative to the equator. But such air-sea interactions favor ITCZ location either northern or southern hemisphere. Why in the real world does the ITCZ favor north of the equator?

3. Idealized GCM experiments

Idealized Numerical Experiments (Li 1997, JAS)

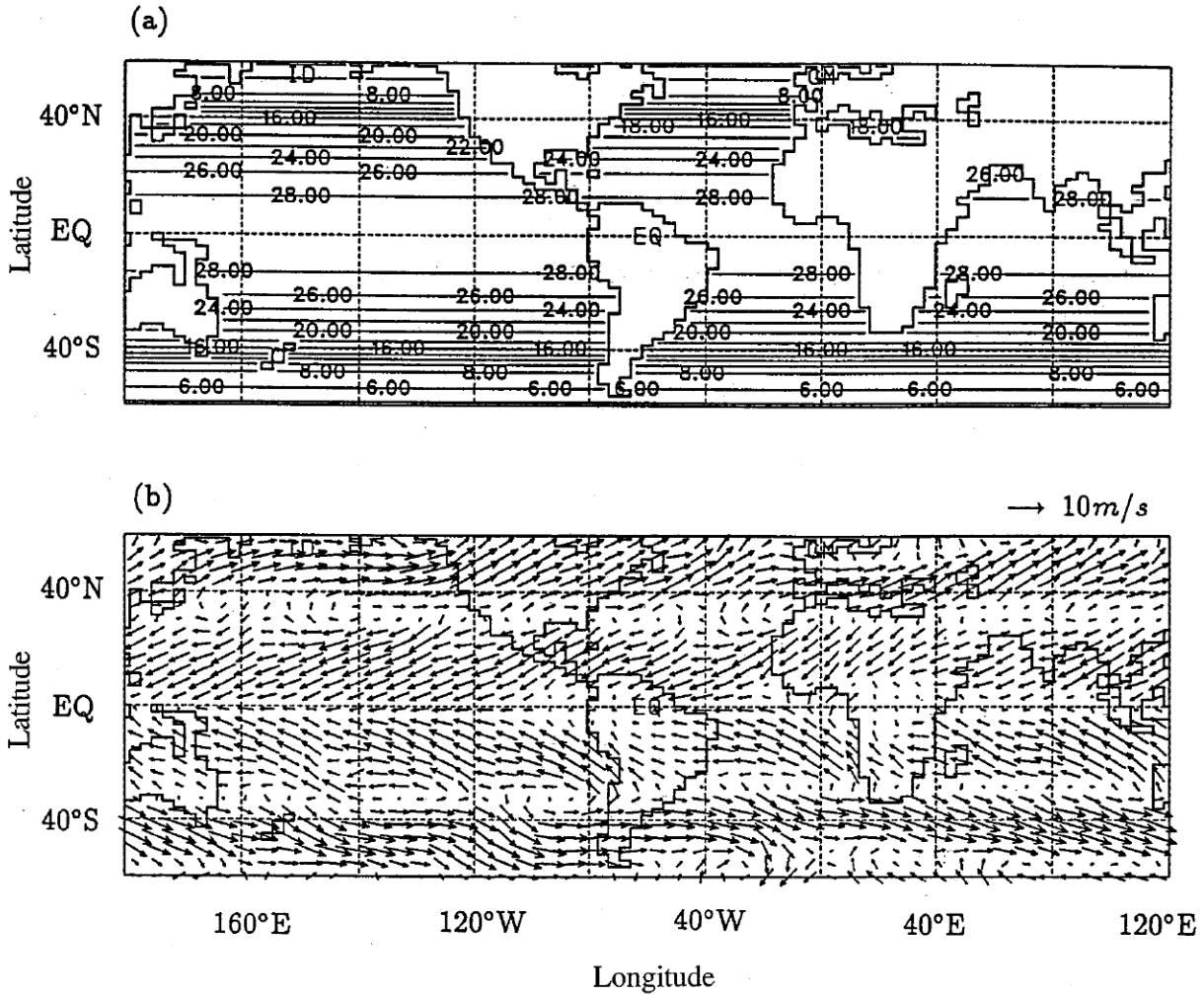

FIG. 9. (a) A prescribed zonal-mean symmetric SST (°C) field derived from the climatological monthly mean COADS dataset (averaged between 140°E and 180°). (b) The R30-model simulated surface wind field forced by the above prescribed symmetric SST and the annual-mean solar radiation.

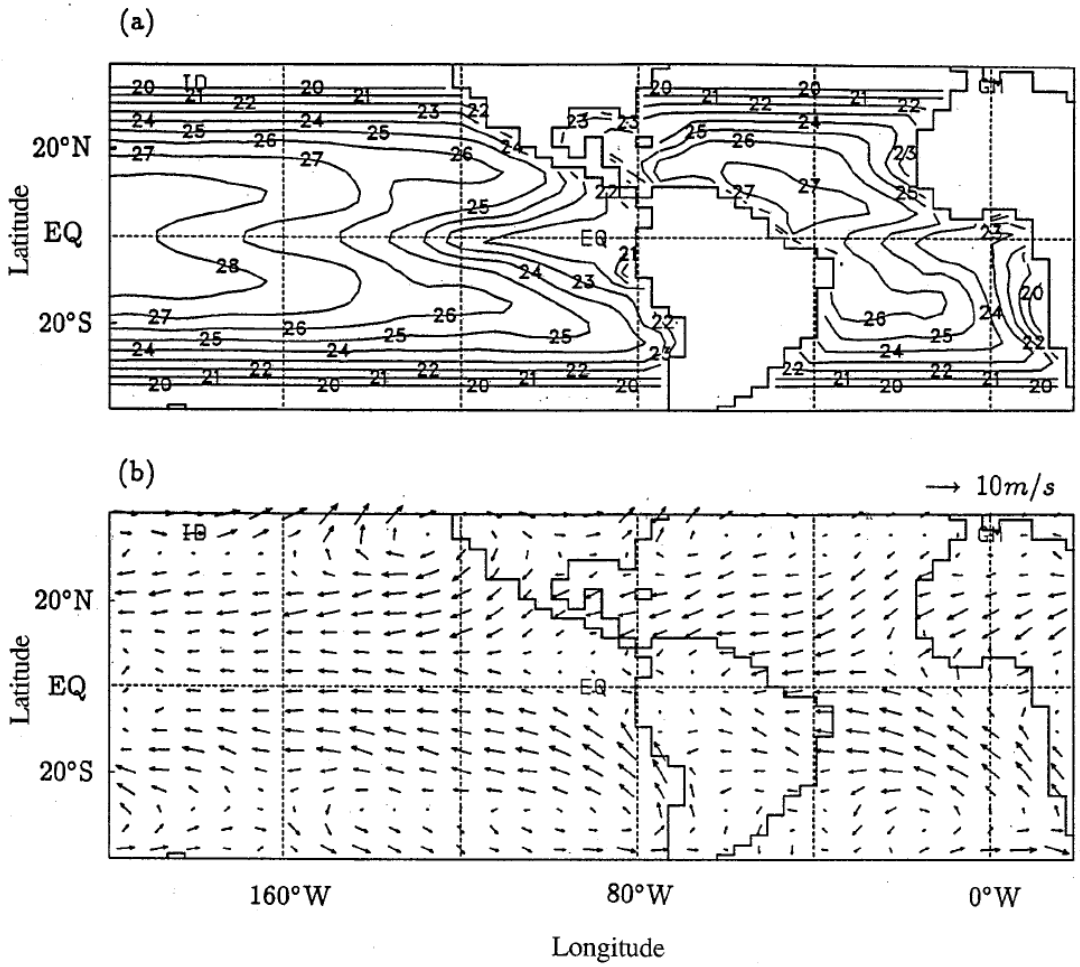

FIG. 10. The simulated (a) SST (°C) and (b) surface wind fields from a hybrid coupled GCM. Only the dynamic coupling is considered in this case. The thermodynamic coupling, such as the surface evaporation and cloud effects, is intentionally suppressed. The model starts from a symmetric SST condition as shown in Fig. 9a.

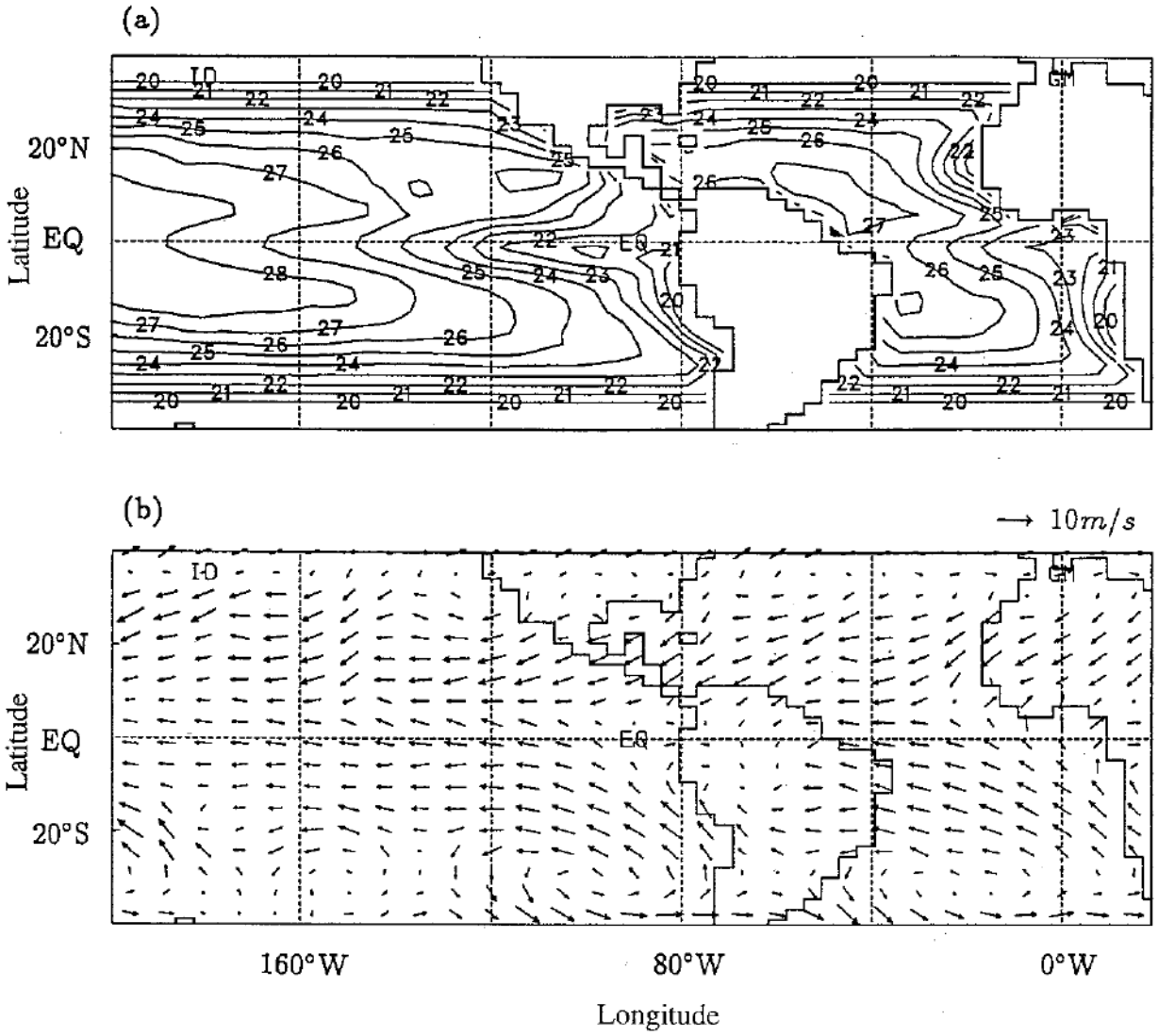

FIG. 12. The simulated (a) SST (°C) and (b) surface wind fields from the hybrid coupled GCM in the presence of the dynamic coupling, the evaporation–wind feedback, and the low-level stratus cloud–SST feedback.

To quantitize the extent of the asymmetry, an equatorial asymmetry index is introduced as

$$A_e = \langle V \rangle (\langle T \rangle_N - \langle T \rangle_S), \tag{3.2}$$

where $\langle V \rangle$ denotes a mean (averaged between 5°S and 5°N) cross-equatorial wind component and $\langle T \rangle_N$ and $\langle T \rangle_S$ stand for, respectively, mean ocean surface temperatures between 10°N and 0° and between 0° and 10°S. The solid line in Fig. 11 shows the index in this case.

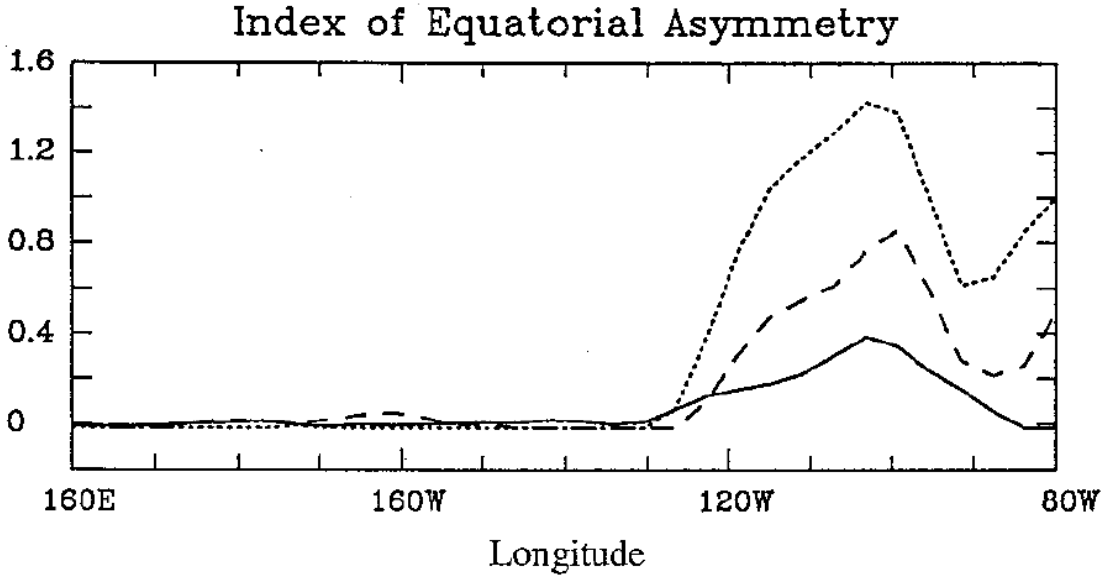

FIG. 11. The longitudinal distribution of the equatorial asymmetry index (°C m s^{-1}) in the three cases: the dynamic coupling (solid line), the dynamic coupling plus the evaporation–wind feedback (dashed line), and the combined dynamic coupling, evaporation–wind feedback, and low-level stratus cloud–SST feedback (dotted line).

Conclusion on ITCZ asymmetry

1. Why is there climatic asymmetry?

   Ocean-Atmosphere interactions favor an anti-symmetric mode.

2. Why does it happens in the eastern Pacific and eastern Atlantic?

   Global Distribution of Continents → regions of monsoons & Trades → Depth of the ocean thermocline

3. Why does the ITCZ stay at north rather than south of the equator?

   Pacific: due to tilting of western coast of Americas

   Atlanic: due to Africa land mass asymmetry

2.2 Mechanism for the annual cycle in the equatorial eastern Pacific

On the Annual Cycle of the Eastern Equatorial Pacific

TIANMING LI AND S. GEORGE H. PHILANDER

Atmospheric and Oceanic Sciences Program, Princeton University, Princeton, New Jersey

(Manuscript received 13 January 1995, in final form 2 May 1995)

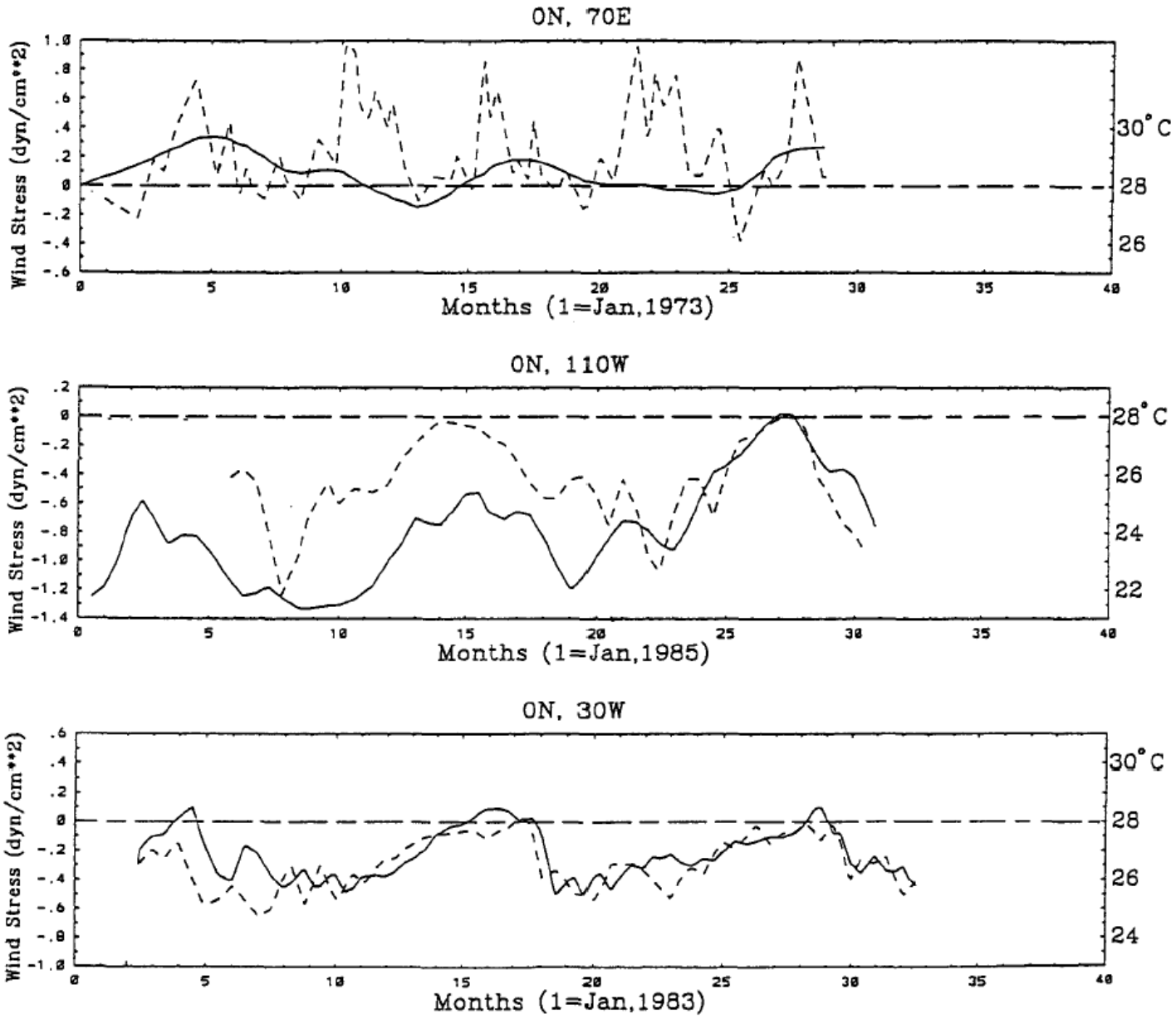

FIG. 1. The time series measurements of sea surface temperature (in °C: solid line) and of the zonal component of the wind stress (in dyn cm^2: dashed line). Time (in units of months) starts on 1 January in all three cases. The first year is (a) 1973 for the measurements at Gan in the Indian Ocean (70°W) by Knox (1981), (b) 1985 for those at 110°W by Halpern (1987) and McPhaden and McCarty (1992), and (c) 1983 for those in the Atlantic at 30°W by Weingartner and Weisberg (1991).

Possible factors that may influence the annual cycle in the equatorial eastern Pacific:

1. Earth's elliptic orbit
2. Tilting of the Earth's axis
3. Equatorial asymmetry of the annual mean state
4. Asymmetry of American coastal geometry

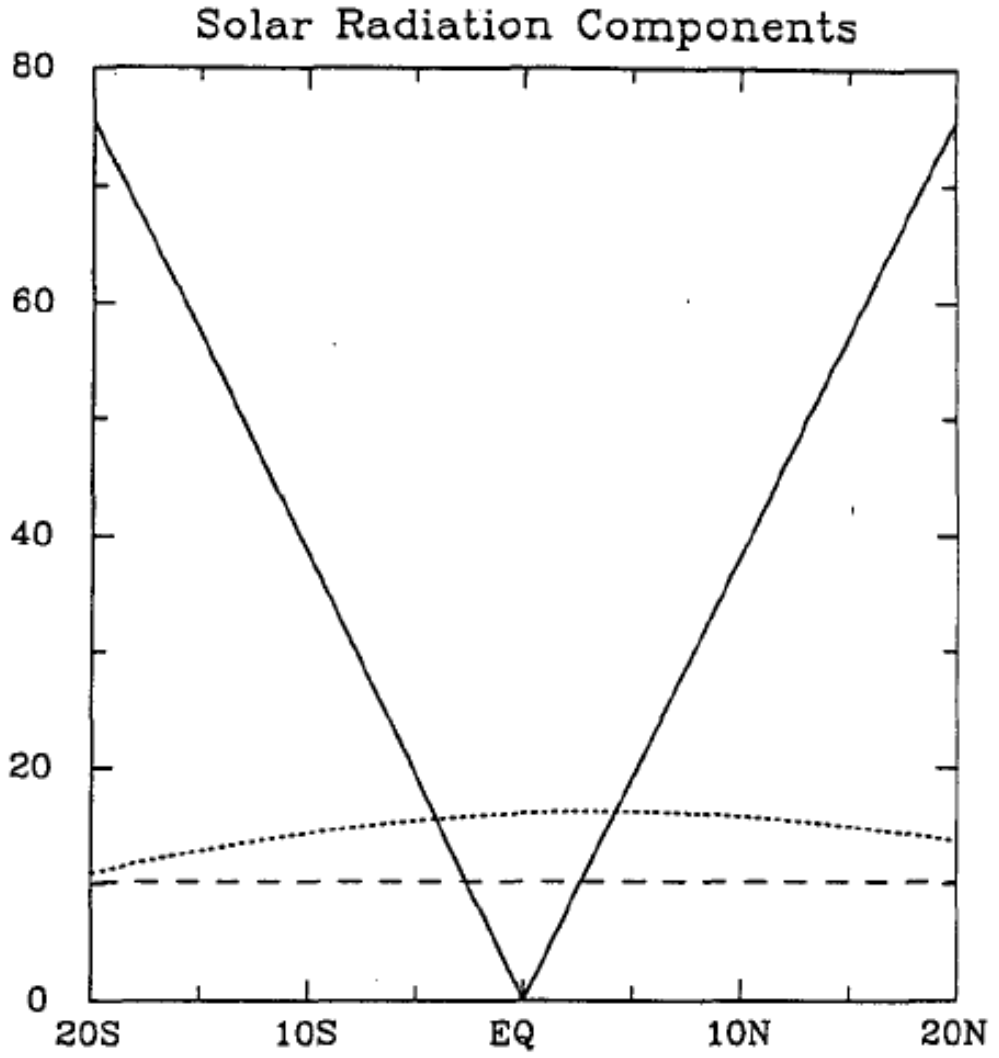

FIG. 6. The latitudinal structure of the amplitude of the antisymmetric annual harmonic (solid line), symmetric annual harmonic (dashed line), and the semiannual harmonic (dotted line) of solar radiation.

Annual Mean SST and Surface Wind

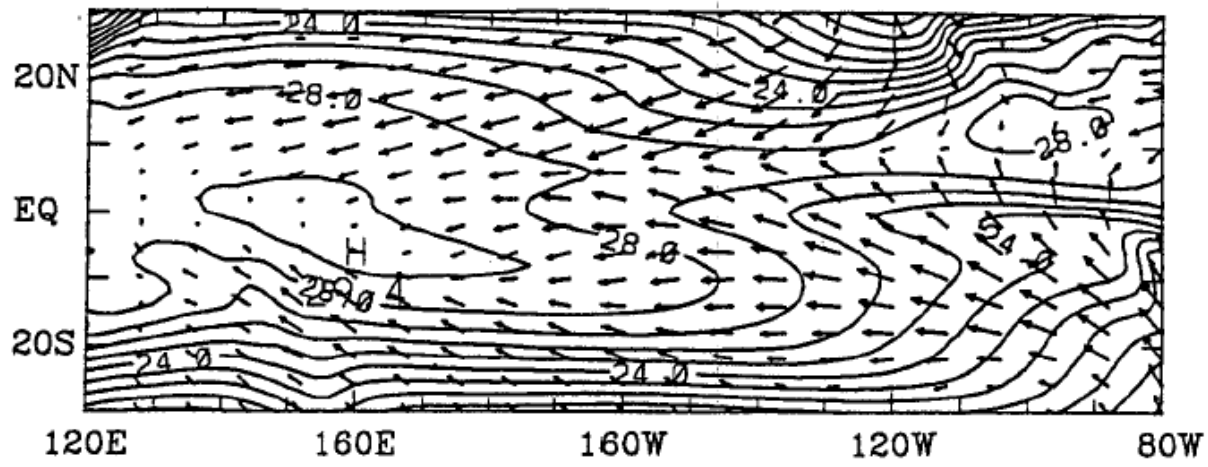

Surface Current and Entrainment Velocity

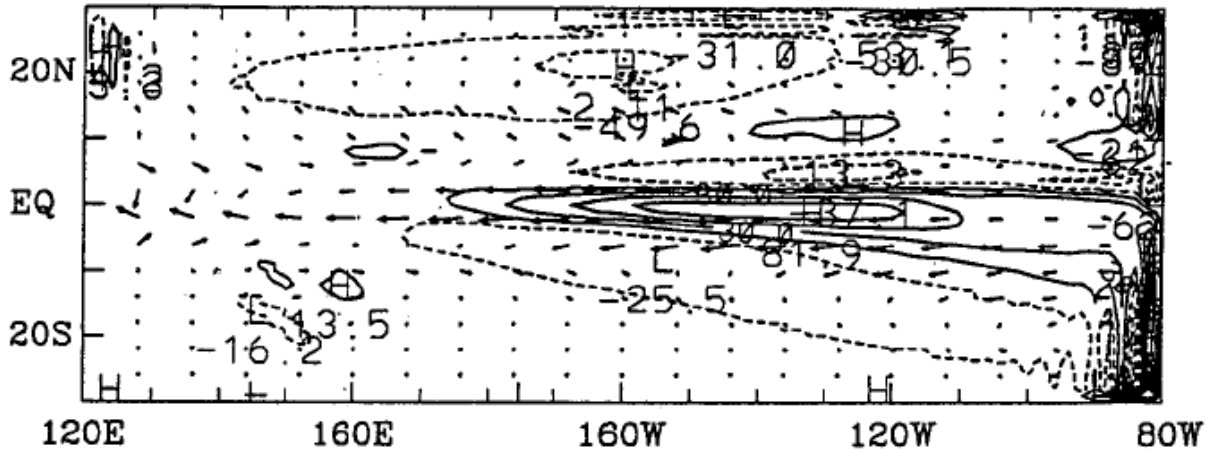

The Ocean model

$$\frac{\partial \mathbf{v}}{\partial t} + f\,\mathbf{k} \times \mathbf{v} = -g'\nabla h + \frac{\boldsymbol{\tau}}{\rho H} - r\mathbf{v} + \nu\nabla^2\mathbf{v} \quad (2.1a)$$

$$\frac{\partial h}{\partial t} + H\nabla \cdot \mathbf{v} = -rh + \kappa\nabla^2 h \quad (2.1b)$$

$$\frac{\partial \tilde{\mathbf{v}}}{\partial t} + f\,\mathbf{k} \times \tilde{\mathbf{v}} = \frac{\boldsymbol{\tau}}{\rho H_1} - r_s\tilde{\mathbf{v}} + \nu\nabla^2\tilde{\mathbf{v}} \quad (2.1c)$$

$$\frac{\partial T}{\partial t} + \mathbf{v}_1 \cdot \nabla(\bar{T} + T) + \overline{\mathbf{v}_1} \cdot \nabla T$$

$$= -[M(\bar{w} + w) - M(\bar{w})]\overline{T_z}$$

$$-M(\bar{w} + w)T_z + \frac{Q}{\rho C_w H_1} - \alpha T + \kappa\nabla^2 T, \quad (2.1d)$$

The sea surface temperature is determined by both the dynamical response of the ocean to the wind

$$\boldsymbol{\tau} = \rho_a C_D[|\mathbf{V} + \bar{\mathbf{V}}|(\mathbf{V} + \bar{\mathbf{V}}) - |\bar{\mathbf{V}}|\bar{\mathbf{V}}] \quad (2.2)$$

The atmospheric model

$$EU - \beta yV = \frac{\partial \phi}{\partial x} + A \frac{\partial T}{\partial x} \qquad (2.3a)$$

$$EV + \beta yU = \frac{\partial \phi}{\partial y} + A \frac{\partial T}{\partial y} \qquad (2.3b)$$

$$\epsilon \phi = -C_0^2 \left(\frac{\partial U}{\partial x} + \frac{\partial V}{\partial y} \right), \qquad (2.3c)$$

SST. Where sea surface temperature is high, convective rather than stratus clouds are likely. In our model the effect of stratus clouds is to reduce the shortwave solar radiation in accord with Reed's (1977) expression

$$Q_{\mathrm{sw}} = [Q_0(1 - 0.62C) - \overline{Q_0}(1 - 0.62\bar{C})](1 - \lambda), \tag{2.4}$$

where Q_0 and $\overline{Q_0}$ represent the total and annual-mean solar radiation at the top of atmosphere; C and $\bar{C}$ denote the total and annual-mean cloudiness; and λ denotes the surface albedo, which is taken to be constant (0.06) in the tropical ocean. In (2.4), we have neglected the effect of noon solar altitude. Separate experiments show this to be an unimportant factor.

Evaporation is calculated from the expression

$$Q_{\mathrm{LH}} = \rho_a C_D L[|\mathbf{V} + \bar{\mathbf{V}}|(q_s - q_a) - |\bar{\mathbf{V}}|(\overline{q_s} - \overline{q_a})], \tag{2.5}$$

where $\rho_a = 1.2$ kg m^{-3} is the surface air density; $C_D = 1.3 \times 10^{-3}$ is a drag coefficient; $L = 2.5 \times 10^6$ J kg^{-1} is the latent heat of vaporization per unit mass; and the total and annual-mean sea surface specific humidities, q_s and $\overline{q_s}$, are computed from the sea surface temperature, based on the Clausius–Clapeyron equa-

March Simulation

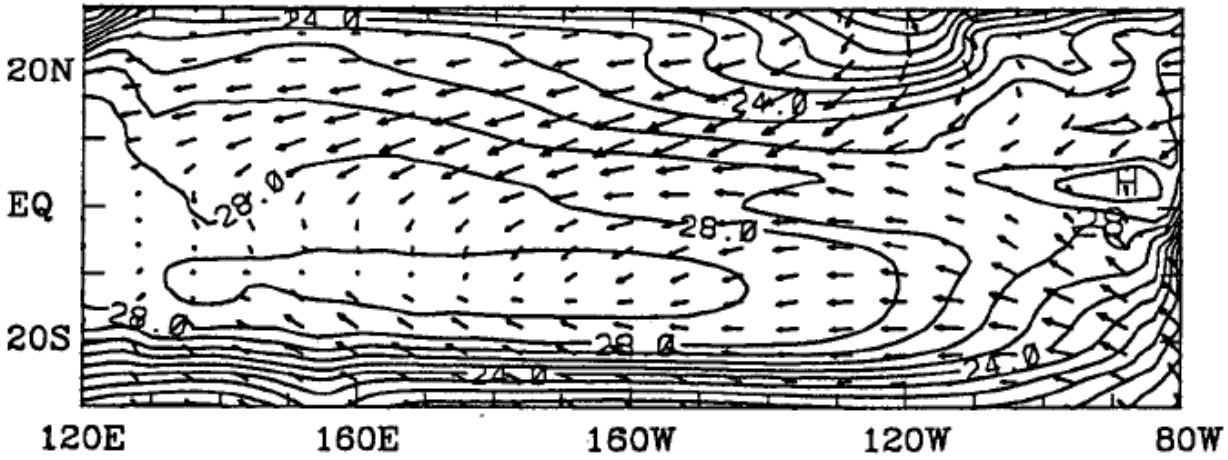

September Simulation

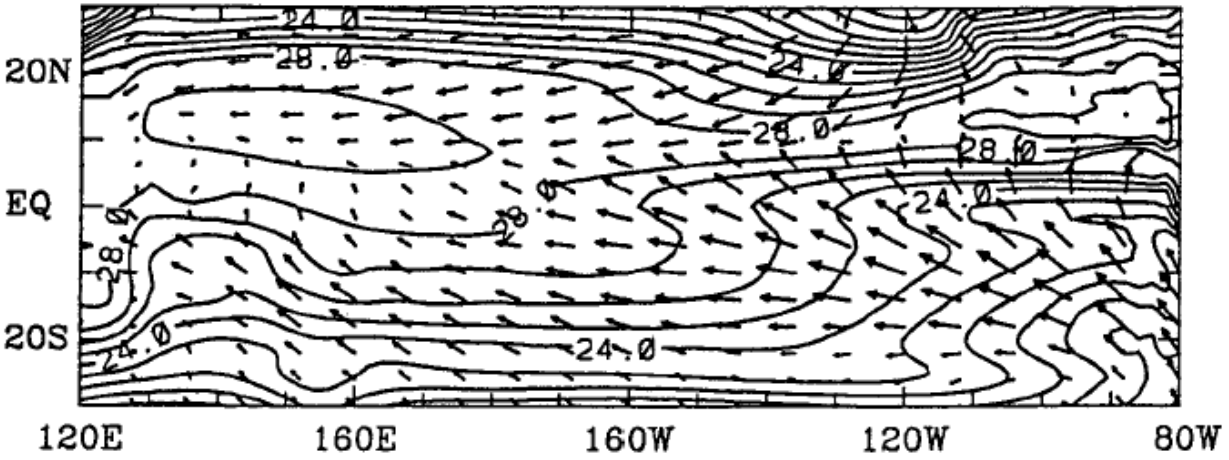

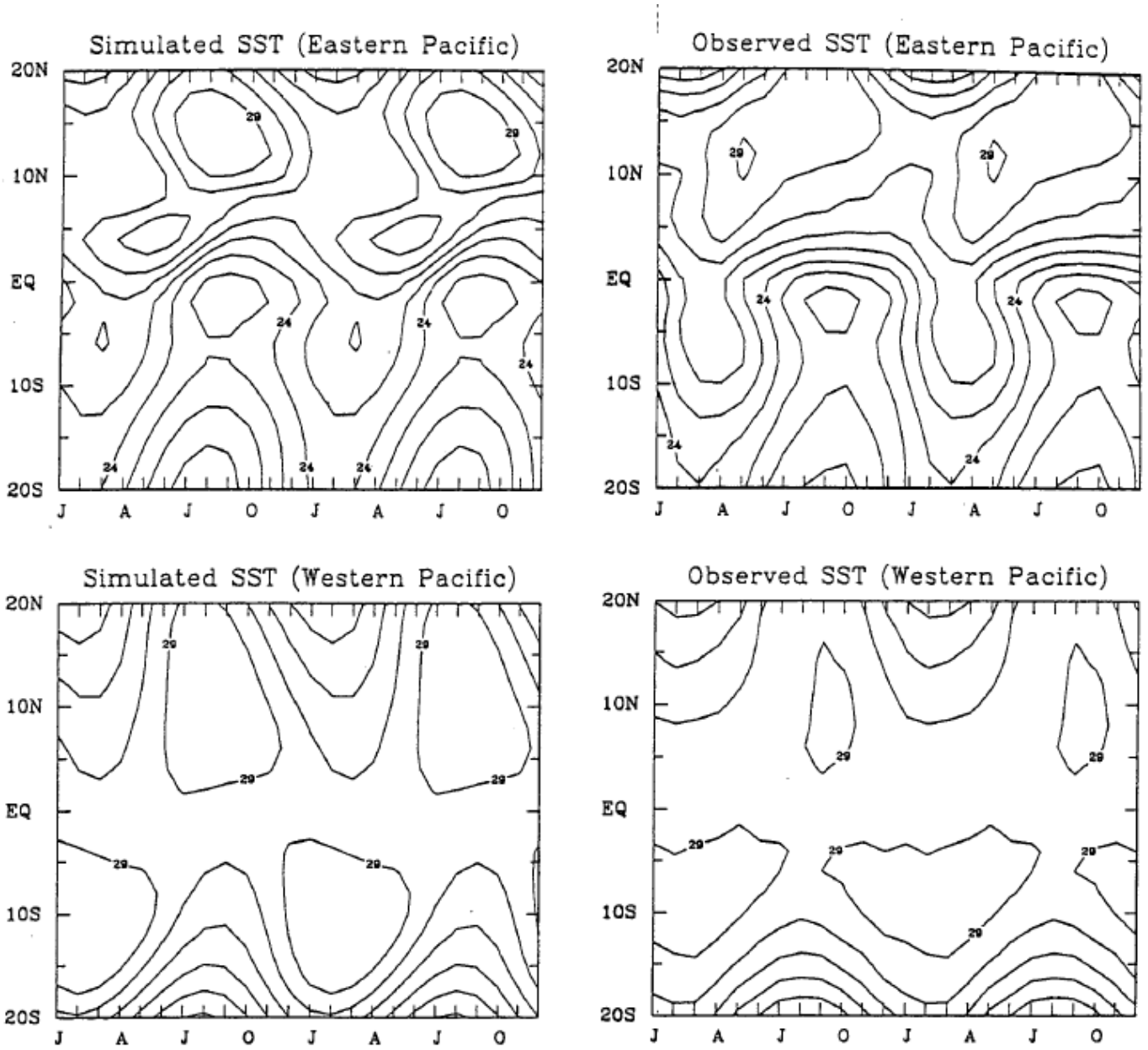

FIG. 4. The annual cycles of sea surface temperatures, simulated and observed, in the eastern Pacific (90°–110°W: upper panels) and in the western Pacific (160°E–180°: lower panels). The model results are from the reference case in which the model is forced with the complete seasonal solar radiation; a realistic, asymmetric annual-mean basic state is specified; and the western coast of the Americas coincides with a meridian.

TABLE 1. Description of model experiments.

Experiment	Description
Reference case	Observed seasonally varying solar radiation; asymmetric time-mean state, rectangular ocean basin, and SST depends on oceanic dynamics and on heat fluxes (including both evaporation and cloud effects).
A	Symmetric annual-harmonic solar radiation, symmetric time-mean state, rectangular ocean basin, and SST as in the reference case.
B	Antisymmetric annual-harmonic solar radiation, symmetric time-mean state, sloping coast in the eastern Pacific, and SST as in the reference case.
C	Antisymmetric annual-harmonic solar radiation, asymmetric time-mean state, rectangular ocean basin, and SST not affected by clouds or evaporation.
D	Antisymmetric annual-harmonic solar radiation, asymmetric time-mean state, rectangular ocean basin, and SST not affected by oceanic dynamics or clouds.
E	Antisymmetric annual-harmonic solar radiation, asymmetric time-mean state, rectangular ocean basin, and SST not affected by clouds.
F	Antisymmetric annual-harmonic solar radiation, asymmetric time-mean state, rectangular ocean basin, and SST as in the reference case.

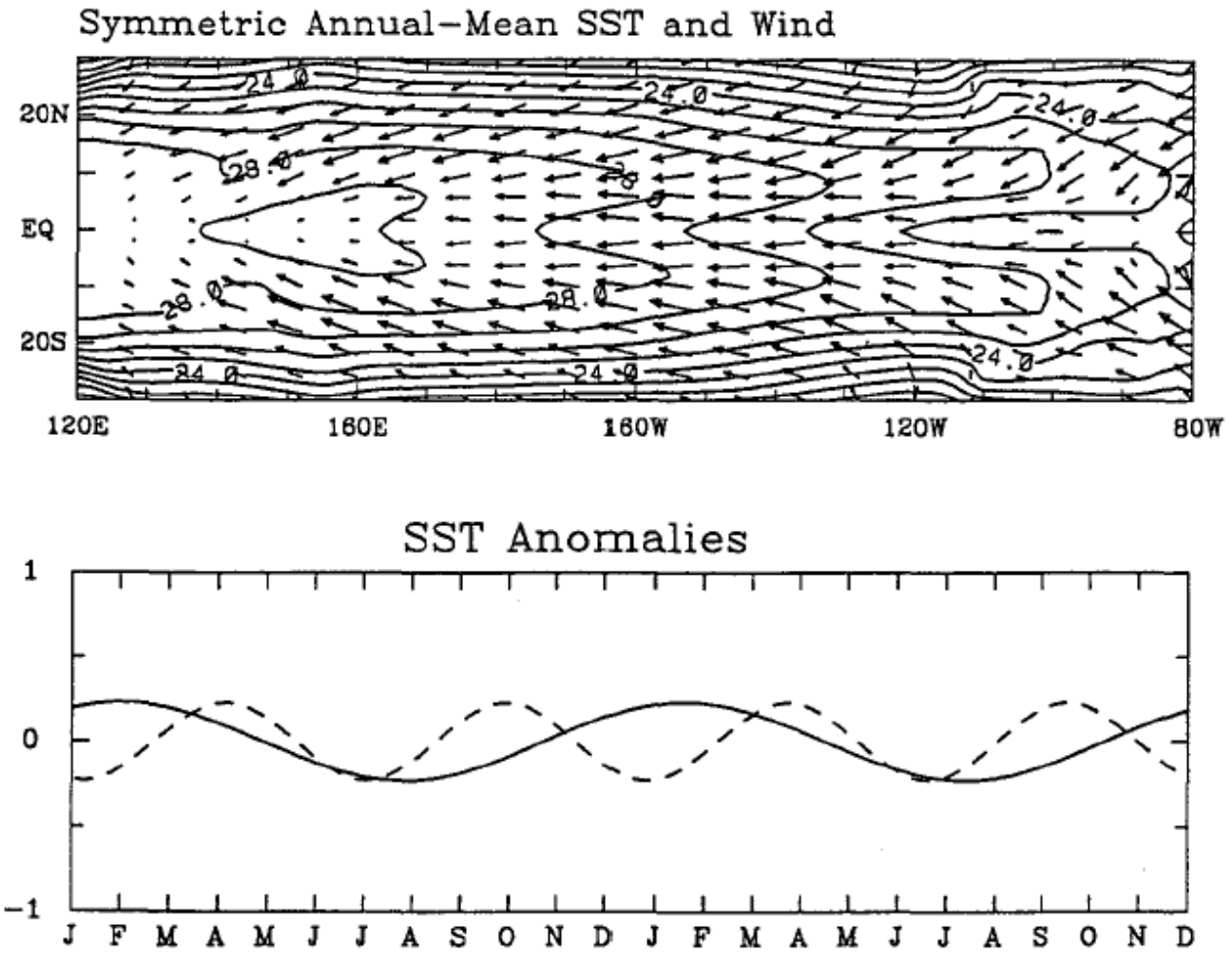

FIG. 5. (a) The symmetric component of climatological annual-mean sea surface temperature and wind fields. (b) The simulated seasonal variations in sea surface temperature at 0°, 100°W from a model forced with the symmetric annual harmonic of the solar radiation (solid line) and with the semiannual harmonic of the solar radiation (dashed line).

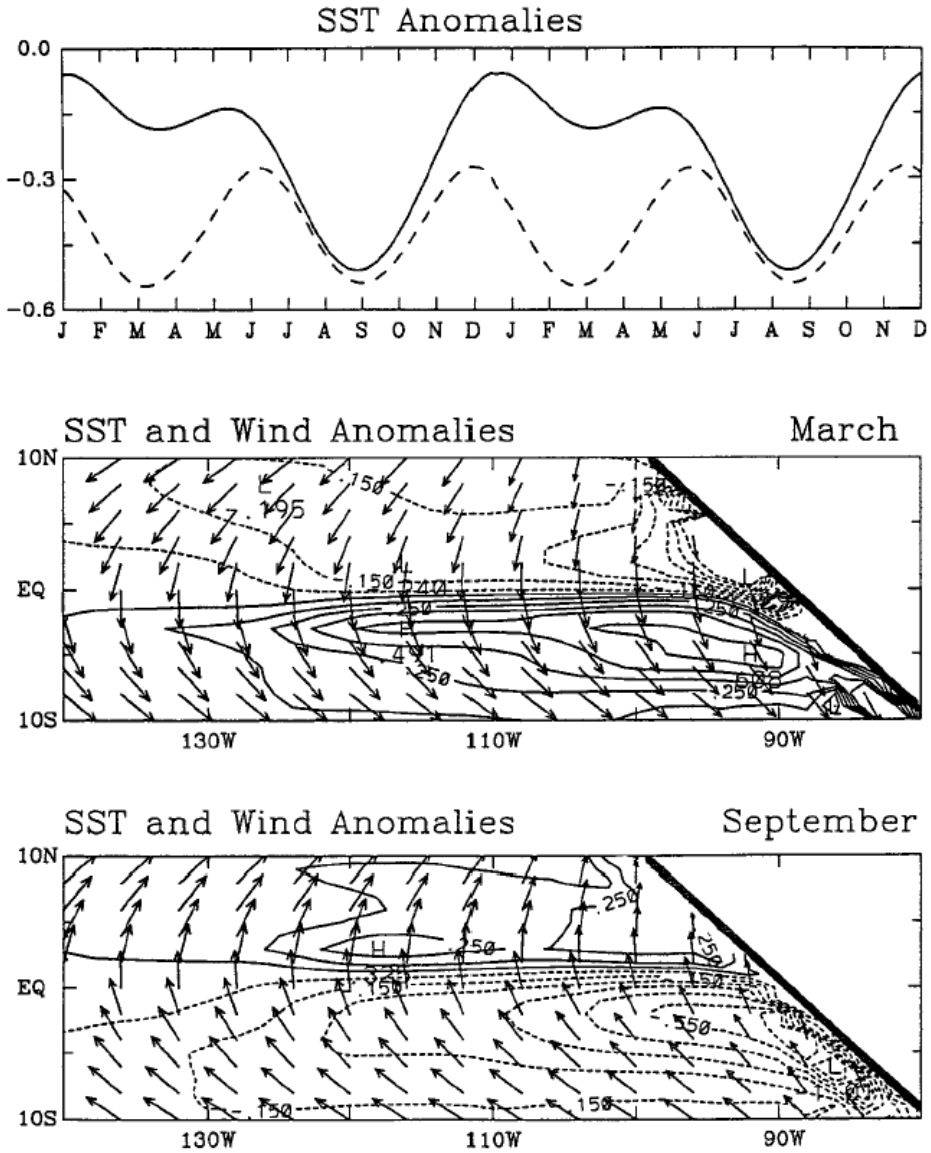

FIG. 7. (a) The time evolution of simulated sea surface temperature anomalies (0°, 100°W) in the presence of a north–south straightline coast (dashed line) and a northwest–southeast sloping coast (solid line). In both cases, a symmetric mean basic state is specified and the forcing is the antisymmetric annual harmonic of solar radiation. The lower panels illustrate the horizontal structure of the anomalous SST and wind fields in (b) March and in (c) September. The maximum wind vector is 1.5 m s^{-1} and the contour interval is 0.1°C.

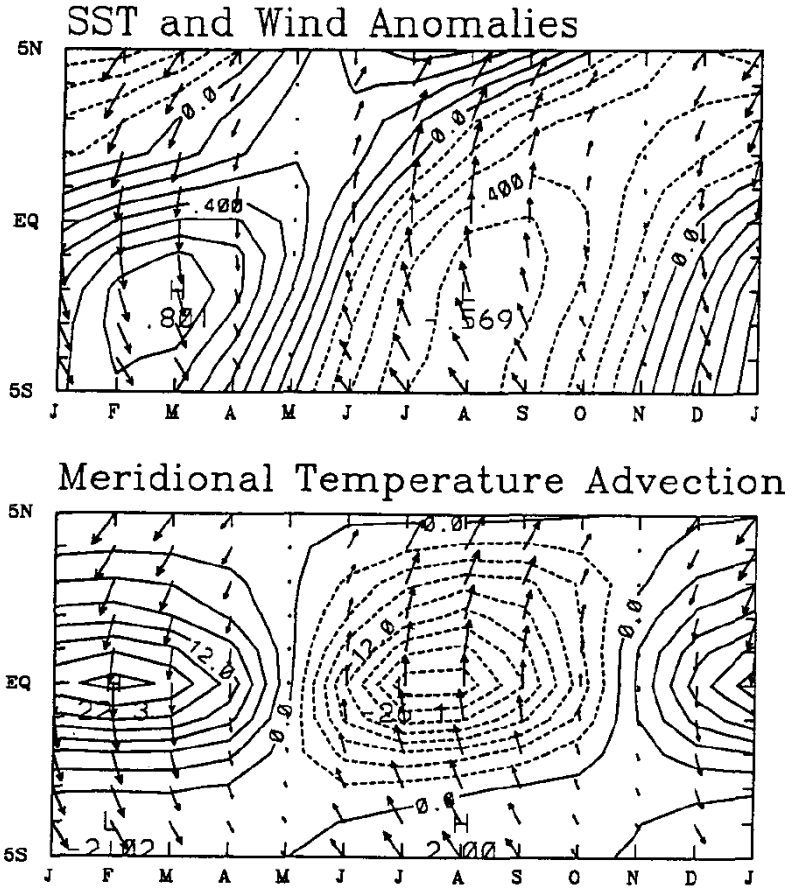

FIG. 8. The time–latitude section of simulated SST and wind anomalies (upper panel) in the eastern Pacific (100°W). In this case, sea surface temperature variations are determined strictly by the dynamic coupling (i.e., wind-induced oceanic upwelling). The thermodynamic coupling, such as latent heat and cloud feedback, is suppressed. The model is forced by a part of solar radiation that is strictly antisymmetric and varies annually. A rectangular ocean boundary is specified. The lower panel shows meridional temperature advection, which converts an antisymmetric SST mode excited by the coupled ocean–atmosphere instability (Chang and Philander 1994) to a symmetric mode and causes the annual change in SST at the equator. The contour intervals are 0.1°C for SST and 3×10^{-8} K s^{-1} for the advection. The maximum wind vector is 2 m s^{-1}.

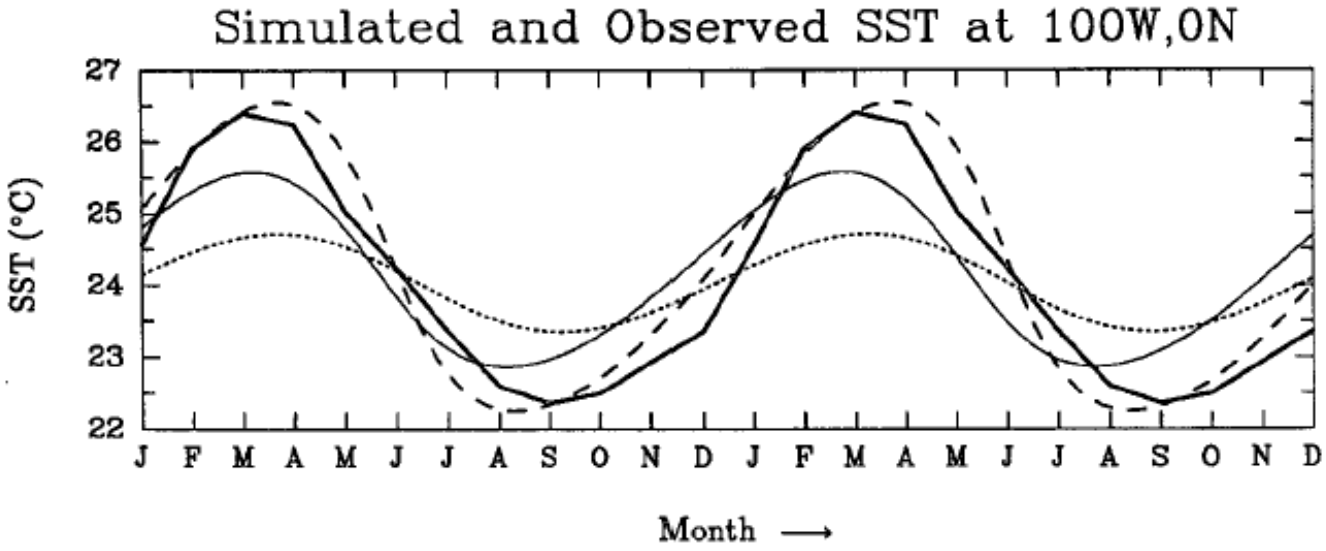

FIG. 9. Seasonal variations of SST at 0°, 100°W in three cases. The SST is determined strictly by evaporation in the case of the dotted line, by evaporation and oceanic upwelling in the case of the solid line, and by evaporation, upwelling, and the presence of low-level stratus clouds in the case of the dashed line. The heavy black line corresponds to the observed variations. In all three cases, a realistic time-mean state that is asymmetric about the equator is specified, the model is forced by part of annually varying solar radiation that is strictly antisymmetric about the equator, and the western coast of the Americas coincides with a meridian.

Conclusion: Mechanism for Annual Cycle at the Equator

1. Anti-symmetric solar radiation forcing is essential.

2. The asymmetric annual mean state is necessary.

3. Three types of air-sea feedback processes (meridional wind-upwelling-SST feedback, wind-evaporation-SST feedback and stratus cloud-radiation-SST feedback) are equally important in causing the annual variation of SST in the eastern equatorial Pacific.